

# Shock Breakout in Type Ibc Supernovae and Application to GRB 060218/SN 2006aj

Li-Xin Li<sup>†</sup>

*Max-Planck-Institut für Astrophysik, 85741 Garching, Germany*

## ABSTRACT

Recently, a soft black-body component was observed in the early X-ray afterglow of GRB 060218, which was interpreted as shock breakout from the thick wind of the progenitor Wolf-Rayet star of the underlying Type Ic SN 2006aj. In this paper we present a simple model for computing the characteristic quantities (including energy, temperature, and time-duration) for the transient event from the shock breakout in Type Ibc supernovae produced by the core-collapse of Wolf-Rayet stars surrounded by dense winds. In contrast to the case of a star without a strong wind, the shock breakout occurs in the wind region rather than inside the star, caused by the large optical depth in the wind. We find that, for the case of a Wolf-Rayet star with a dense wind, the total energy of radiation generated by the supernova shock breakout is larger than that in the case of the same star without a wind by a factor  $\gtrsim 10$ . The temperature can be either hotter or cooler, but the time-duration is always larger caused by the increase in the effective radius of the star due to the presence of a thick wind. Then, we apply the model to SN 2006aj. We show that, the energy released by the shock breakout is too small to explain the black-body component observed in GRB 060218, unless that the progenitor star has an unrealistically large core radius (the radius at optical depth of 20), larger than  $80R_{\odot}$ . Despite this disappointing result, our model is expected to have important applications to the observations on Type Ibc supernovae in which the detection of shock breakout will provide important clues to the progenitors of SNe Ibc.

## Key words:

shock waves – supernovae: general – supernovae: individual: SN 2006aj – gamma-rays: bursts – stars: Wolf-Rayet – stars: winds, outflow.

## 1 INTRODUCTION

Since the first detection of the afterglows (Costa et al. 1997; van Paradijs et al. 1997; Frail et al. 1997) and host galaxies (Bloom et al. 1998, 1999; Fruchter et al. 1999b) of gamma-ray bursts (GRBs), by now it has well been established that long-duration GRBs are cosmological events occurring in star-forming galaxies (Paczyński 1998a; Fruchter et al. 1999a; Berger, Kulkarni & Frail 2001; Frail et al. 2002; Christensen, Hjorth & Gorosabel 2004; Sollerman et al. 2005; Fruchter et al. 2006, and references therein), and are most likely produced by the core-collapse of massive stars (Woosley, Heger & Weaver 2002; Piran 2004; Zhang & Mészáros 2004; Woosley & Heger 2006a, and references therein). This scenario has got strong support from the cumulative evidence that some, if not all, long-duration GRBs are associated with supernovae (SNe), either from direct observations of supernova features in the spectra of

GRB afterglows, or from indirect observations of rebrightening and/or flattening (called “red bumps”) in GRB afterglows which are interpreted as the emergence of the underlying SN lightcurves (Della Valle 2006; Woosley & Heger 2006b, and references therein). The discovery of the connection between GRBs and SNe has been one of the most exciting developments in the fields of GRBs and SNe in the past decade.

Interestingly, all the SNe that have been spectroscopically confirmed to be associated with GRBs, including SN 1998bw/GRB 980425 (Galama et al. 1998), SN 2003dh/GRB 030329 (Stanek et al. 2003; Hjorth et al. 2003b), SN 2003lw/GRB 031203 (Malesani et al. 2004), and the most recent one, SN 2006aj/GRB 060218 (Masetti et al. 2006; Modjaz et al. 2006; Campana et al. 2006; Sollerman et al. 2006; Pian et al. 2006; Mirabal et al. 2006; Cobb et al. 2006), are Type Ic showing no detectable hydrogen and helium lines. However, the SNe associated with GRBs also remarkably differ from ordinary Type Ibc SNe: they have extremely smooth and featureless spectra

<sup>†</sup> E-mail: lxl@mpa-garching.mpg.de

indicating very large expansion velocity, are much more energetic (i.e., involving much larger explosion energy), and eject significantly larger amount of nickels (Hamuy 2004; Della Valle 2006; Woosley & Heger 2006b), except SN 2006aj/GRB 060218 which is somewhat closer to normal SNe Ibc (see below) (Mazzali et al. 2006). For these reasons, they are often called “hypernovae” to be distinguished from normal SNe (Paczyński 1998a,b; Iwamoto 1998).

The discovery of GRB-SN connection has provided us important clues to the progenitors of GRBs, since it is broadly believed that Type Ibc supernovae are produced by the core-collapse of Wolf-Rayet (WR) stars who have lost their hydrogen (possibly also helium) envelopes due to strong stellar winds or interaction with a companion (Smartt et al. 2002; Woosley, Heger & Weaver 2002; Filippenko 2004; Woosley & Heger 2006a, and references therein). In fact, for several GRBs, observations with high quality optical spectra have identified the presence of highly ionized lines with high relative velocities most likely coming from shells or clumps of material from WR stars, supporting WR stars as GRB progenitors (Mirabal et al. 2003; Schaefer et al. 2003; Klose et al. 2004; Chen, Prochaska & Bloom 2006, see, however, Hammer et al. 2006).

A systematic study on the GRB afterglows by Zeh, Klose & Hartmann (2004) suggested that all long-duration GRBs are associated with SNe. However, it appears that only a small fraction of Type Ic SNe are able to produce GRBs, since the rate of GRBs and hypernovae are several orders of magnitude lower than the rate of core-collapse SNe (Podsiadlowski et al. 2004). Although both long-duration GRBs and core-collapse SNe are found in star-forming galaxies, their location in the hosts and the morphology and luminosities of their host galaxies are significantly different as most clearly revealed by the recent study of Fruchter et al. (2006) with *Hubble Space Telescope* (*HST*) imaging. The core-collapse SNe trace the blue-light of their hosts that are approximately equally divided between spiral and irregular galaxies, while long GRBs are far more concentrated on the brightest regions of faint and irregular galaxies. Fruchter et al. (2006) argued that their results may be best understood if GRBs are formed from the collapse of *extremely massive* and *low-metallicity* stars.

The preference of long GRBs to low-metallicity galaxies (Fynbo et al. 2003; Hjorth et al. 2003a; Le Floc'h et al. 2003; Sollerman et al. 2005; Fruchter et al. 2006) has been strengthened by the recent paper of Stanek et al. (2006), in which a strong anti-correlation between the isotropic energy of the four nearby SN-connected GRBs and the oxygen abundance in their host galaxies was found, which was used to argue that the life in the Milky Way is protected away from GRBs by metals. Stanek et al. (2006) have suggested that long GRBs do not trace star formation, but trace the metallicity.

The discovery of GRB 060218 and its association with SN 2006aj by *Swift* has shed more light on the GRB-SN connection as well as on the nature of GRBs. GRB 060218 has a cosmological redshift  $z = 0.0335$  corresponding to a distance 145Mpc with  $H_0 = 70\text{km s}^{-1}\text{Mpc}^{-1}$ , which makes it the second nearest GRB among those having determined redshifts (about four times the distance of GRB 980425 at  $z = 0.0085$ ) (Campana et al. 2006; Pian et al.

2006; Sollerman et al. 2006). This GRB is very unusual in several aspects. It has an extremely long duration, about 2100 s. Its spectrum is very soft, with an photon index  $2.5 \pm 0.1$  and peak energy  $E_{\text{peak}} = 4.9_{-0.3}^{+0.4}\text{ keV}$  in the GRB frame. The isotropic equivalent energy is  $E_{\text{iso}} = (6.2 \pm 0.3) \times 10^{49}\text{ ergs}$  extrapolated to the 1 – 10,000 keV in the rest frame energy band (Campana et al. 2006), which is at least 100 times fainter than normal cosmological GRBs but among a population of under-energetic GRBs (Sazonov, Lutovinov & Sunyaev 2004; Liang, Zhang & Dai 2006).

Although the SN associated with GRB 060218, i.e. SN 2006aj, is broadly similar to those previously discovered GRB-connected SNe, it also shows some remarkable unusual features compared to them (Pian et al. 2006; Sollerman et al. 2006; Mazzali et al. 2006). Among the four GRB-connected SNe mentioned above, SN 2006aj is the faintest one, although still brighter than normal Type Ibc SNe. Its lightcurve rises more rapidly, and its expansion velocity indicated by the spectrum is intermediate between that of other GRB-connected SNe and that of normal SNe Ibc. Modeling of the lightcurve of SN 2006aj reveals that SN 2006aj is much less energetic compared to other GRB-connected SNe: it had an explosion energy  $E_{\text{in}} \approx 2 \times 10^{51}\text{ ergs}$ , ejected a mass  $M_{\text{ej}} \approx 2M_{\odot}$ , compared to  $E_{\text{in}} \sim 3 - 6 \times 10^{52}\text{ ergs}$ , and  $M_{\text{ej}} \sim 10M_{\odot}$  of the others (Mazzali et al. 2006). This suggests that SN 2006aj is somewhat closer to normal Type Ibc SNe, and there does not exist a clear gap between hypernovae and normal SNe.

The X-ray afterglow observation by the X-Ray Telescope (XRT) on board *Swift* on GRB 060218 started 159 s after the burst trigger. A very interesting feature of the early X-ray afterglow is that it contains a soft black-body component which has a temperature about 0.17 keV and comprises about 20% of the total X-ray flux in the 0.3 – 10 keV range, lasting from 159 s up to  $\sim 10,000$  s. The black-body component was not detected in later XRT observations (Campana et al. 2006). The total energy contained in this component, as estimated by Campana et al., is  $\sim 10^{49}\text{ ergs}$ . They interpreted it as SN shock breakout from a dense wind surrounding the progenitor WR star of the supernova.

Butler (2006) conducted an analysis on the early X-ray afterglows of a sample ( $> 70$ ) of GRBs observed by XRT/*Swift*. He found that although most of the afterglow spectra can be fitted with a pure power law with extinction, a small fraction of them show appreciable soft thermal components at 5 – 10% level. His reanalysis on GRB 060218 shows that the black-body component contains energy as much as  $2.3 \times 10^{50}\text{ ergs}$ , but lasts only  $\sim 300$  s. In fact, the soft black-body component dominates the flux after  $\sim 1,000$  s from the burst trigger according to his analysis.

Brilliant flashes from shock breakout in SNe was first predicted by Colgate (1968) almost forty years ago, originally proposed for GRBs that had not been discovered yet. However, it has not been unambiguously detected in supernova observations yet (Calzavara & Matzner 2004). This is mainly due to the transient nature of the event. It is generally expected that the flash from shock breakout precedes the supernova, is much brighter and harder and than the supernova but has a very short time-duration.

For the famous Type II SN 1987A, theoretical calculations have shown that the shock emergence from the surface

of the progenitor (Sk 1, a blue supergiant) would have produced a radiation of  $\sim 10^{47}$  ergs in the EUV to soft X-ray band, lasting 1–3 minutes (Imshennik & Nadézhin 1988, 1989; Enzman & Burrows 1992; Blinnikov et al. 2000). In fact, in the observed bolometric lightcurve of SN 1987A, there was a fast initial decline phase which could be the tail of the lightcurve produced by the shock breakout (Imshennik & Nadézhin 1989). If the shock breakout interpretation of the soft black-body component in GRB 060218 is confirmed, it would have important impact on the theories of both GRBs and SNe.

Although the propagation of a strong shock and the appearance of shock emergence (breakout) in supernovae have been intensively studied both analytically and numerically (Klein & Chevalier 1978; Imshennik & Nadézhin 1988, 1989; Enzman & Burrows 1992; Blinnikov et al. 1998, 2000, 2002; Matzner & McKee 1999; Tan, Matzner & McKee 2001), in the situation of SNe produced from stars with dense stellar winds they have not been fully explored yet. If the stellar wind of the progenitor is very optically thick—which is indeed the case for Type Ibc SNe whose progenitors are believed to be WR stars—the shock breakout will occur in the wind region after the shock passes through the surface of the star, in stead of in the region inside the star. Since a stellar wind has a mass density profile that is very different from that of a star, the model that has been developed for the shock emergence in SNe with progenitors without consideration of stellar winds cannot be directly applied to the case with dense stellar winds.

In this paper, we present a simple model for semi-analytically computing the propagation of a strong shock in a dense stellar wind, and estimating the characteristic quantities for the transient events from the shock breakout in SNe Ibc. The model is obtained by extending the existing model of shock breakout for SNe without consideration of stellar winds. Then, we apply the model to SN 2006aj and examine if the soft black-body component in the early X-ray afterglow of GRB 060218 is consistent with SN shock breakout interpretation.

The paper is organized as follows. In Sec. 2, we describe a simple but general model for the mass density and velocity profile for winds around WR stars. In Sec. 3, we model the propagation of a supernova shock in a stellar wind, taking into account the relativistic effects. In Sec. 4, we analyze the evolution of the shock front, and the radiation energy contained in it. In Sec. 5, we present a procedure for calculating the quantities characterizing the transient events arising from the shock breakout, including the released energy, the temperature, and the time-duration. In Sec. 6, we present the numerical results. In Sec. 7, we apply our model to SN 2006aj/GRB 060218. In Sec. 8, we summarize our results and draw our conclusion.

Appendix A is devoted to the formulae for computing the optical depth of a wind in the framework of the standard stellar wind model. Appendix B presents the formulae for computing the characteristic quantities for SN shock breakout from a star without winds, in the trans-relativistic regime.

## 2 MASS DENSITY PROFILE OF THE WINDS OF WOLF-RAYET STARS

Wolf-Rayet stars are very luminous, hot, and massive stars that are nearly at the end of their stellar lives. Based on their spectra, WR stars are often classified as WN stars (nitrogen dominant) and WC stars (carbon dominant). WR stars are characterized by extremely dense stellar winds, losing mass at a rate of  $10^{-6} - 10^{-4} M_{\odot}/\text{yr}$  with wind terminal velocity of 700–3,000 km/s. The mass lost from WR stars by stellar winds is so enormous that most (if not all) of hydrogens of WR stars have been lost. This is a main reason for the belief that WR stars are the progenitors of Type Ibc supernovae.

Some basic relations between physical parameters of WR stars can be found in Langer (1989); Schaerer & Maeder (1992); Nugis & Lamers (2000).

The wind of a WR star is usually extremely dense. This is characterized by the fact that, for the majority of WR stars, the ratio of the momentum of the wind ( $\dot{M}v_{\infty}$ , where  $\dot{M}$  is the mass-loss rate,  $v_{\infty}$  is the terminal velocity of the wind) to the momentum of radiation ( $L/c$ , where  $L$  is the luminosity of the star,  $c$  is the speed of light) is much larger than unity, indicating that on average each photon leaving the star must be scattered several times and the wind must be optically thick. As a result, the photospheric radius ( $R_{\text{ph}}$ , defined by the radius where the optical depth  $\tau = 2/3$ ) often differs from the core radius of the star ( $R_{\star}$ , defined to be the radius where  $\tau = 20$ ) by a factor  $\gtrsim 2$ .

In Fig. 1, we plot the photospheric radius against the core radius for 86 Galactic WC and WN-type stars (Hamann, Koesterke & Wessolowski 1995; Koesterke & Hamann 1995) and 6 LMC WC-type stars (Gräfener et al. 1998), determined with the “standard model” of stellar winds. For many WRs, especially those of WC-type, we have  $R_{\text{ph}} \gtrsim 2R_{\star}$ .

From the parameters of the 92 Galactic and LMC WR stars, a correlation between  $\dot{M}R_{\star}/v_{\infty}$  and  $R_{\text{ph}}$  can be derived. Let us define a mass function

$$\begin{aligned} \Psi &\equiv \frac{\dot{M}R_{\star}}{v_{\infty}} \\ &= 1.654 \times 10^{-9} M_{\odot} \left( \frac{\dot{M}}{5 \times 10^{-5} M_{\odot} \text{ yr}^{-1}} \right) \left( \frac{R_{\star}}{3R_{\odot}} \right) \\ &\quad \times \left( \frac{v_{\infty}}{2000 \text{ km s}^{-1}} \right)^{-1}. \end{aligned} \quad (1)$$

In Fig. 2, we plot  $\log \Psi$  against  $\log R_{\text{ph}}$  for the 92 WRs. Clearly, there is a strong correlation between  $\Psi$  and  $R_{\text{ph}}$ , which is best fitted by

$$\log \Psi = -10.87 + 2.36 \log R_{\text{ph}} \quad (2)$$

for all stars, and

$$\log \Psi = -10.42 + 1.77 \log R_{\text{ph}} \quad (3)$$

for WC stars only, where  $\Psi$  is in units of  $M_{\odot}$ , and  $R_{\text{ph}}$  is in units of  $R_{\odot}$ .

The mass density of a steady and spherically symmetric wind is related to the mass-loss rate and the wind velocity by

$$\rho(r) = \frac{\dot{M}}{4\pi r^2 v_r(r)}, \quad (4)$$

where  $r$  is the radius from the center of the star, and

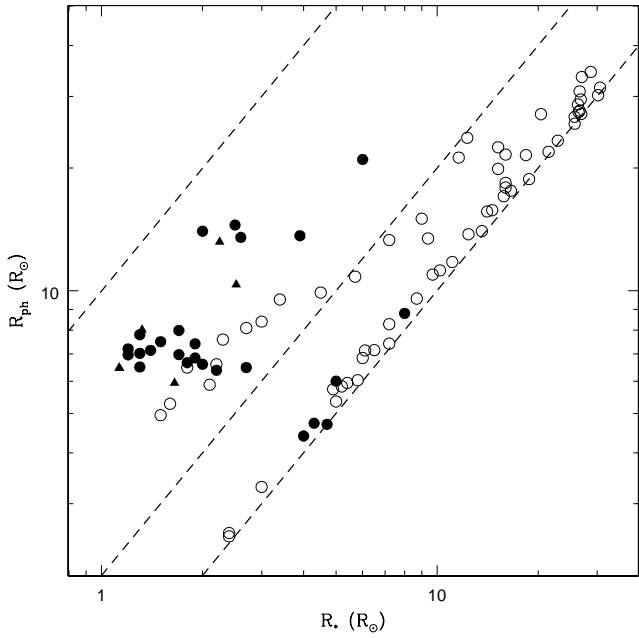


**Figure 1.** Photospheric radius versus stellar core radius, for 86 Galactic WRs (filled circles for WC-type, open circles for WN-type) and 6 LMC WRs (triangles, WC-type only). The dashed lines show the relation of  $R_{\text{ph}} = R_{\star}$ ,  $R_{\text{ph}} = 2R_{\star}$ , and  $R_{\text{ph}} = 10R_{\star}$ .

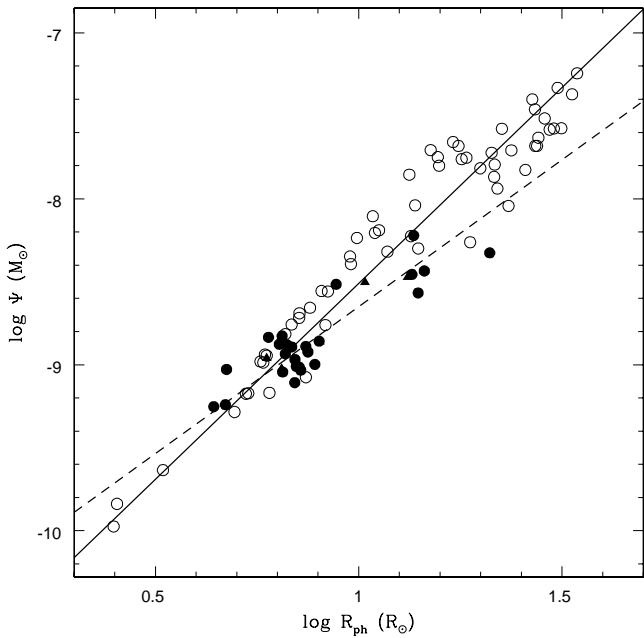


**Figure 2.** The mass function  $\Psi$  defined by eq. (1) against the photospheric radius for the sample of WRs in Fig. 1. Clearly there is a strong correlation between  $\Psi$  and  $R_{\text{ph}}$ . The solid straight line is the best fit to all the data by eq. (2). The dashed straight line is the best fit to the WC stars (filled symbols) by eq. (3).

$v_r$  is the wind velocity. We model the velocity of the wind by (Schaerer 1996; Ignace, Oskinova & Foulon 2000; Nugis & Lamers 2002)

$$v_r(r) = v_{\infty} \left(1 - \frac{\alpha R_{\star}}{r}\right)^b, \quad (5)$$

where  $\alpha < 1$  and  $b \geq 1$  are free parameters. The presence of  $\alpha$  in equation (5) is to ensure that the mass density of the wind is regular at the stellar radius  $r = R_{\star}$ . Although in the “standard model” of WR winds the value of  $b$  is usually adopted to be unity as in the case of O-stars, it has been argued that for WR stars  $b$  can be significantly larger (Robert 1994; Schmutz 1997; Lépine & Moffat 1999). According to the model of Nugis & Lamers (2002),  $b$  is typically in the range of 4–6.

The value of  $\alpha$  can be determined by the radial velocity of the wind at the stellar radius. If we define  $\varepsilon = v_{\star}/v_{\infty}$ , where  $v_{\star} \equiv v_r(R_{\star})$ , then

$$\alpha = 1 - \varepsilon^{1/b}. \quad (6)$$

Typically,  $v_{\star}$  has the order of the sound speed at  $R_{\star}$ , and  $\varepsilon \sim 0.01$  (Schaerer 1996).

In the outer wind region, where  $r \gg R_{\star}$ , the wind density  $\rho \sim r^{-2}$ . In the region close to the stellar surface (i.e.,  $r \sim R_{\star}$ ), the wind density has a much steeper slope. As will be seen in Sec. 3, it is this very steep mass density profile near the surface of the star that accelerates the shock in the wind region.

The opacity in the WR wind region is usually very complex and generally a function of radius (Nugis & Lamers 2002; Gräfener & Hamman 2005). Here we approximate it by a constant opacity  $\kappa$ . The optical depth of the wind is then

$$\tau \equiv \int_r^{\infty} \kappa \rho dr = \frac{A}{(b-1)\alpha R_{\star}} \left[ \left(1 - \frac{\alpha}{y}\right)^{1-b} - 1 \right], \quad (7)$$

where  $y \equiv r/R_{\star}$  and  $A \equiv \kappa \dot{M}/(4\pi v_{\infty})$ .

As commonly adopted in the literature, we define the stellar core radius  $R_{\star}$  to be the radius where  $\tau = 20$ . Then, we can write the optical depth as

$$\tau = \tau_0 \left[ \left(1 - \frac{\alpha}{y}\right)^{1-b} - 1 \right], \quad (8)$$

where

$$\tau_0 \equiv \frac{A}{(b-1)\alpha R_{\star}} = \frac{20}{(1-\alpha)^{1-b} - 1}. \quad (9)$$

By definition, the boundary of the photosphere is at the photospheric radius where  $\tau = 2/3$ . Then, we can solve for  $y_{\text{ph}} \equiv R_{\text{ph}}/R_{\star}$  from equation (8)

$$y_{\text{ph}} = \alpha \left[ 1 - \left(1 + \frac{2}{3\tau_0}\right)^{1/(1-b)} \right]^{-1}. \quad (10)$$

For given  $b$ ,  $y_{\text{ph}}$  is a decreasing function of  $\alpha$ . As  $\alpha \rightarrow 1$ , we have  $\tau_0 \rightarrow 0$  and  $y_{\text{ph}} \rightarrow 1$ . As  $\alpha \rightarrow 0$ , we have  $\tau_0 \approx 20/[(b-1)\alpha]$  and  $y_{\text{ph}} \rightarrow 30$ . Thus, in general we must have  $1 < y_{\text{ph}} < 30$ . By equation (6),  $\alpha$  is a decreasing function of  $\varepsilon$ .

From  $\tau(y = y_{\text{ph}}) = 2/3$  and the definition of  $A$ , we can

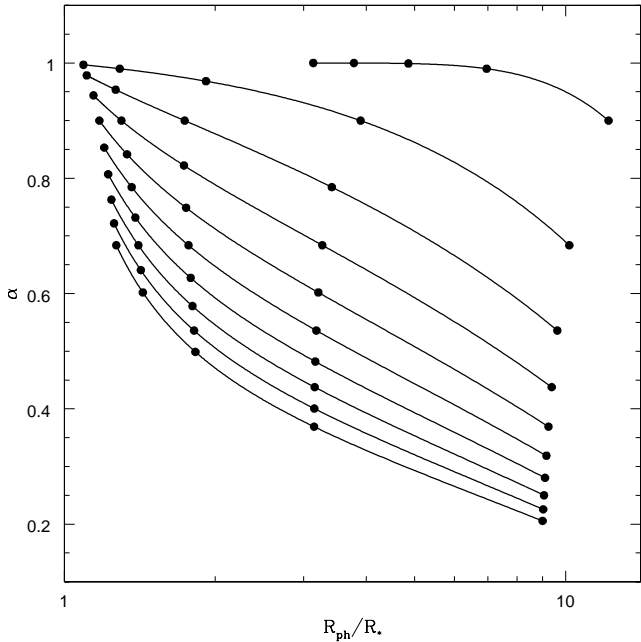


**Figure 3.** The solution for  $\alpha$  and  $y_{\text{ph}} = R_{\text{ph}}/R_{\star}$ , for  $\varepsilon = 10^{-5} - 10^{-1}$ . Top to bottom:  $b = 1 - 10$  with  $\Delta b = 1$ . The filled circles on each curve label the values of  $\varepsilon = 10^{-5}, 10^{-4}, 10^{-3}, 10^{-2}, 10^{-1}$  from left to right.

derive the “surface density” of the stellar wind

$$\Sigma \equiv \frac{\dot{M}}{4\pi v_{\infty} R_{\text{ph}}} = \frac{2}{3\kappa} \frac{\alpha(b-1)}{y_{\text{ph}} \left[ (1 - \alpha/y_{\text{ph}})^{1-b} - 1 \right]} . \quad (11)$$

This equation can be used to eliminate  $\dot{M}$  and  $v_{\infty}$  from the equations for the shock breakout (Sec. 5).

The above results for the optical depth and the surface density are valid only for  $b > 1$ . The corresponding formulae for  $b = 1$  are given in Appendix A.

In Fig. 3, we plot  $\alpha$  versus  $y_{\text{ph}}$ , solved from equations (6) and (10) (or eq. A3 when  $b = 1$ ) for a set of discrete values of  $b$  (from 1 to 10) and continuous values of  $\varepsilon$  (from  $10^{-5}$  to  $10^{-1}$ ). The value of  $y_{\text{ph}}$  sensitively depends on  $\varepsilon$ . For the same value of  $b$ ,  $y_{\text{ph}}$  drops quickly as  $\varepsilon$  decreases. When  $\varepsilon$  is fixed,  $y_{\text{ph}}$  decreases if  $b$  increases from  $b = 1$ , very fast for small values of  $\varepsilon$ . However, for  $b > 3$ , the effect of the variation in  $b$  on the value of  $y_{\text{ph}}$  is not dramatic.

### 3 PROPAGATION OF A STRONG SHOCK WAVE IN THE WIND

The propagation of a strong shock wave in a gas is determined by two competing processes: the shock is decelerated by collecting mass from the ambient gas, and accelerated by the steep downward gradient of the gas mass density (if the steep downward gradient exists). After the shock has collected enough mass and the total mass contained in the shocked region does not change any more, the behavior of the shock is essentially determined by the profile of the mass density in the region that the shock is plowing into (see, e.g., Matzner & McKee 1999). Then, for a spherically symmetric gas, the shock is accelerated when  $d(\rho r^3)/dr < 0$ , and decelerated when  $d(\rho r^3)/dr > 0$ . Gnatyk (1985) suggested

a formula for the shock momentum for both non-relativistic and relativistic shocks

$$\Gamma_s \beta_s \propto (\rho r^3)^{-\alpha_g} , \quad (12)$$

where  $\beta_s$  is the speed of the shock front divided by the speed of light,  $\Gamma_s \equiv (1 - \beta_s^2)^{-1/2}$  is the Lorentz factor,  $\alpha_g = 0.5$  for decelerating, and  $\alpha_g = 0.2$  for accelerating shocks.

Although equation (12) quite accurately describes both the limits of non-relativistic ( $\beta_s^2 \ll 1$ ) and ultra-relativistic ( $\Gamma_s \gg 1$ ) shocks, Tan, Matzner & McKee (2001) have shown that it is not accurate in the trans-relativistic case ( $\beta_s$  close to 1 but  $\Gamma_s$  not large enough). Based on their numerical results and the work of Matzner & McKee (1999), Tan, Matzner & McKee (2001) suggested the following formula for both non-relativistic and trans-relativistic shocks (but not for ultra-relativistic shocks)

$$\begin{aligned} \Gamma_s \beta_s &= p (1 + p^2)^{0.12} , \\ p &\equiv 0.736 \left( \frac{E_{\text{in}}}{mc^2} \right)^{1/2} \left( \frac{\rho r^3}{m} \right)^{-0.187} , \end{aligned} \quad (13)$$

for accelerating shocks. In equation (13),  $E_{\text{in}}$  is the explosion kinetic energy,  $m(r) \equiv M(r) - M_{\text{rem}}$ ,  $M_{\text{rem}}$  is the mass of the material that will become the SN remnant, and  $M(r)$  is the mass of the material contained in radius  $r$ . At the radius where shock breakout takes place (either inside the star but close to its surface, or in the wind region), we have  $m \approx M_{\text{ej}}$ , where  $M_{\text{ej}}$  is the ejected mass.

Because the compactness of WR stars, the problem that we are solving here is right in the trans-relativistic regime (as will be confirmed latter in this paper). Thus we will use equation (13) to calculate the momentum of accelerating shocks.

A shock wave propagating in a wind with a density given by equations (4) and (5) is accelerated in the region near the stellar surface  $r = R_{\star}$ , but decelerated at large radius since  $\rho \propto r^{-2}$  for  $r \gg R_{\star}$ . The transition from acceleration to deceleration occurs at a radius determined by  $d(\rho r^3)/dr = 0$ , where the shock velocity reaches the maximum. The transition radius is found to be

$$R_a = (1 + b)\alpha R_{\star} . \quad (14)$$

After passing the transition radius, the shock starts decelerating, for which we adopt equation (12) with  $\alpha_g = 1/2$  to describe the motion of the shock wave. Then

$$\Gamma_s \beta_s \propto (\rho r^3)^{-1/2} \quad (15)$$

when  $r > R_a$ , which is  $\propto r^{-1/2}$  when  $r \gg R_{\star}$ .

The maximum  $\Gamma_s \beta_s$  is then obtained by submitting  $r = R_a$  into equation (13)

$$\mathcal{G}_{\text{max}} \equiv (\Gamma_s \beta_s)_{\text{max}} = p_{\text{max}} (1 + p_{\text{max}}^2)^{0.12} , \quad (16)$$

where

$$\begin{aligned} p_{\text{max}} &= 1.181 [\alpha f(b)]^{-0.187} \left( \frac{E_{\text{in}}}{M_{\text{ej}} c^2} \right)^{1/2} \left( \frac{\Psi}{M_{\text{ej}}} \right)^{-0.187} , \\ f(b) &\equiv (1 + b) \left( 1 + \frac{1}{b} \right)^b , \end{aligned} \quad (17)$$

where the mass function  $\Psi$  is defined by equation (1).

Submitting fiducial numbers in, we get

$$p_{\max} = 1.137\mu \left[ \frac{\alpha f(b)}{f(5)} \right]^{-0.187} \left( \frac{E_{\text{in}}}{10^{52} \text{ergs}} \right)^{0.5} \times \left( \frac{M_{\text{ej}}}{10M_{\odot}} \right)^{-0.313} \left( \frac{R_{\star}}{3R_{\odot}} \right)^{-0.187}, \quad (18)$$

where

$$\mu \equiv \left( \frac{\dot{M}}{5 \times 10^{-5} M_{\odot} \text{yr}^{-1}} \right)^{-0.187} \left( \frac{v_{\infty}}{2000 \text{km s}^{-1}} \right)^{0.187}. \quad (19)$$

Thus, typically the shock is trans-relativistic.

Before passing through the critical radius  $R_a$ , the shock accelerates according to equation (13), where  $m \approx M_{\text{ej}}$ . After passing through the critical radius, the shock enters the deceleration region where we have

$$\Gamma_s \beta_s \approx \mathcal{G}_{\max} \left( \frac{\rho r^3}{\rho_a R_a^3} \right)^{-1/2}, \quad (20)$$

where

$$\rho_a = \frac{f(b)\dot{M}}{4\pi(1+b)R_a^2 v_{\infty}} \quad (21)$$

is the mass density at  $r = R_a$ .

#### 4 THE ENERGY OF RADIATION CONTAINED IN THE SHOCK FRONT

The gas pressure behind the relativistic shock front, measured in the frame of the shocked gas, is (Blandford & McKee 1976)

$$p_2 = (\gamma_2 - 1)(\hat{\gamma}_2 \gamma_2 + 1)\rho c^2, \quad (22)$$

where  $\hat{\gamma}_2$  is the polytropic index of the shocked gas,  $\gamma_2$  is the Lorentz factor of the shocked gas, and  $\rho$  is the mass density of the unshocked gas. The Lorentz factor  $\gamma_2$  is related to the Lorentz factor of the shock front  $\Gamma = \Gamma_s$  by the equation (5) of Blandford & McKee (1976). Since WR winds are radiation-dominated, we have  $\hat{\gamma}_2 = 4/3$ . Then, we can approximate  $p_2$  by

$$p_2 \approx F_p(\Gamma_s v_s) \rho \Gamma_s^2 v_s^2, \quad (23)$$

where  $F_p(\Gamma_s v_s) \sim 1$  is defined by

$$F_p(x) \equiv \frac{2}{3} + \frac{4}{21(1+0.4252x)^{0.4144}}, \quad (24)$$

which has the correct asymptotic values as  $\Gamma_s v_s \rightarrow \infty$  (ultra-relativistic limit) and  $\Gamma_s v_s \rightarrow 0$  (non-relativistic limit), and has a fractional error < 0.3% in the trans-relativistic regime.

Denoting the temperature of the radiation behind the shock front by  $T_2$ , then the pressure of the radiation is

$$\frac{1}{3}aT_2^4 \approx p_2 \approx F_p(\Gamma_s v_s) \rho \Gamma_s^2 v_s^2, \quad (25)$$

measured in the frame of the shocked gas.

A strong shock has a very narrow front. In the non-relativistic limit, the geometric thickness of the shock front is  $\Delta r_s \approx c/(\kappa \rho v_s)$ , the mean free path of photons multiplied by the optical depth of the shock (Imshennik & Nadézhin 1988, 1989)

$$\tau_s = \frac{c}{v_s}. \quad (26)$$

In the ultra-relativistic limit, the thickness of the shock front in the rest frame is  $\propto \Gamma_s^{-2}$  (Blandford & McKee 1976). Hence, using the optical depth of the shock and that of the wind, we can estimate the geometric thickness of the shock front in the rest frame by

$$\Delta r_s \approx \xi \frac{\tau_s}{\tau} \frac{r}{\Gamma_s^2}, \quad (27)$$

where

$$\xi \equiv \frac{\tau}{\kappa \rho r} = \left| \frac{\partial \ln \tau}{\partial \ln r} \right|^{-1} = \frac{y}{\alpha(b-1)} \left[ 1 - \frac{\alpha}{y} - \left( 1 - \frac{\alpha}{y} \right)^b \right]. \quad (28)$$

The function  $\xi(y)$  increases with  $y$ . As  $y \rightarrow \infty$ , we have  $\xi \rightarrow 1$ . As  $y \rightarrow \alpha$ , we have  $\xi \rightarrow 0$ . (When  $b = 1$ ,  $\xi$  is given by eq. A5 in Appendix A.)

The total energy of the radiation contained in the shock front, measured in the frame of the shocked gas, is

$$E_R \approx \frac{1}{3} (aT_2^4) 4\pi r^2 (\gamma_2 \Delta r_s) \approx \frac{4\pi \tau_s \gamma_2}{3\tau \Gamma_s^2} \xi (aT_2^4) r^3, \quad (29)$$

where the factor 1/3 accounts for the fact that the energy density is not uniform and concentrated at the boundary of the shock, and the factor  $\gamma_2$  accounts for the Lorentz contraction. Submitting equation (25) into equation (29), we get

$$E_R \approx \frac{4\pi \tau_s \gamma_2}{\tau \Gamma_s^2} \xi F_p(\Gamma_s v_s) \rho r^3 \Gamma_s^2 v_s^2. \quad (30)$$

Using the definition of  $\xi$ , we have

$$E_R \sim \frac{4\pi \gamma_2 c}{\Gamma_s^2 \kappa v_s} F_p r^2 \Gamma_s^2 v_s^2 \propto r^2 \Gamma_s v_s,$$

since  $F_p \sim 1$  and  $\gamma_2/\Gamma_s \sim 1$ .

In the accelerating region ( $r < R_a$ ),  $\Gamma_s v_s$  and  $\gamma_2$  increase with  $r$ . Hence, the total energy contained in the shock front as measured by the rest observer,  $\gamma_2 E_R$ , increases with  $r$ .

In the decelerating region ( $r > R_a$ ), by equation (15) we have  $\Gamma_s v_s \propto r^{-1/2}$ , thus  $E_R \propto r^{3/2}$ . In the non-relativistic limit,  $\gamma_2 E_R \propto r^{3/2}$ . In the ultra-relativistic limit,  $\gamma_2 E_R \propto \gamma_2 r^{3/2} \propto r$  since  $\gamma_s = \Gamma_s/\sqrt{2} \propto r^{-1/2}$  (Blandford & McKee 1976). Thus, in the region of  $r > R_a$ , we also expect that the total energy contained in the shock front,  $\gamma_2 E_R$ , increases with  $r$  although the shock is decelerating. This is caused by the fact that the volume contained in the shock front increases with  $r$ .

#### 5 EMERGENCE OF THE SHOCK AND CHARACTERISTIC QUANTITIES

Inside the star and deep inside the wind, photons have a diffusion velocity that is slower than the velocity of the shock front caused by the large optical depth of the gas, so that the radiation generated by the shock is trapped and moves with the shock front. As the shock approaches the boundary of the photosphere the optical depth of the gas decreases, until a radius is reached where the diffusion velocity of photons exceeds the velocity of the shock.

Thus, the shock emerges at a radius where the optical

depth of the gas is equal to the optical depth of the shock

$$\tau \approx \frac{c}{v_s}, \quad (31)$$

since beyond that radius photons diffuse faster than the shock front moves (Imshennik & Nadézhin 1988, 1989; Matzner & McKee 1999). Since  $v_s < c$  always, the shock must emerge at a radius where  $\tau > 1$ , inside the photosphere. The maximum breakout radius is at

$$y_{\max} = \alpha \left[ 1 - \left( 1 + \frac{1}{\tau_0} \right)^{1/(1-b)} \right]^{-1}, \quad (32)$$

which occurs when  $v_s \rightarrow c$  and  $\tau \rightarrow 1$  (i.e., in the ultra-relativistic limit).

When  $y < y_a \equiv R_a/R_\star$  (i.e.,  $r < R_a$ ),  $\Gamma_s \beta_s$  is determined by equation (13), which can be recast into

$$\begin{aligned} \Gamma_s \beta_s &= p (1 + p^2)^{0.12}, \\ p &= 1.181 \left( \frac{E_{\text{in}}}{M_{\text{ej}} c^2} \right)^{1/2} \left( \frac{\Psi}{M_{\text{ej}}} \right)^{-0.187} \\ &\quad \times y^{-0.187} \left( 1 - \frac{\alpha}{y} \right)^{-0.187b}, \end{aligned} \quad (33)$$

where  $\Psi$  is defined by equation (1).

When  $y > y_a$  (i.e.,  $r > R_a$ ),  $\Gamma_s \beta_s$  is determined by equation (20), which can be recast into

$$\Gamma_s \beta_s \approx \mathcal{G}_{\max} [\alpha f(b)]^{1/2} y^{-1/2} \left( 1 - \frac{\alpha}{y} \right)^{b/2}. \quad (34)$$

With equations (33), (34), and (8) (or A1 when  $b = 1$ ), we can calculate the radius where the shock breakout takes place,  $R_{\text{br}} \equiv y_{\text{br}} R_\star$ , by numerically solving the algebraic equation (31).

After solving for  $y_{\text{br}}$ , we can obtain the momentum of the shock at  $y = y_{\text{br}}$ , by equations (33) and (34).

Since the shock breakout occurs at a radius where  $\tau_s \approx \tau$  (eq. 31), by equation (30) the total energy of the radiation generated by the shock emergence is

$$E_{\text{br}} \equiv [\gamma_2 E_R]_{r=R_{\text{br}}} \approx 4\pi \xi F_\gamma^2 F_p \rho r^3 \Gamma_s v_s^2 \Big|_{r=R_{\text{br}}}, \quad (35)$$

where  $F_p = F_p(\Gamma_s v_s) \sim 1$ ,  $F_\gamma = F_\gamma(\Gamma_s) \equiv \gamma_2/\Gamma_s \sim 1$ . The Lorentz factors  $\gamma_2$  and  $\Gamma_s$  are related by the equation (5) of Blandford & McKee (1976). For the case of  $\hat{\gamma} = 4/3$ ,  $F_\gamma$  can be approximated by

$$F_\gamma(x) \approx \frac{1}{\sqrt{2}} + \frac{1 - 1/\sqrt{2}}{[1 + 0.9572(x - 1)]^{0.9325}},$$

which gives the correct asymptotic values at the non-relativistic limit ( $\Gamma_s \rightarrow 1$ ) and the ultra-relativistic limit ( $\Gamma_s \rightarrow \infty$ ), and has a fractional error  $< 0.08\%$  in the trans-relativistic case.

At  $y = y_{\text{br}}$ , the energy can be evaluated by

$$\begin{aligned} E_{\text{br}} &\approx \Psi c^2 [\xi F_\gamma^2 F_p \Gamma_s^2 \beta_s^2]_{y=y_{\text{br}}} y_{\text{br}} \left( 1 - \frac{\alpha}{y_{\text{br}}} \right)^{-b} \\ &\approx 1.48 \times 10^{46} \text{ ergs} \left( \frac{\dot{M}}{5 \times 10^{-5} M_\odot \text{ yr}^{-1}} \right) \left( \frac{R_\star}{3R_\odot} \right) \\ &\quad \times \left( \frac{v_\infty}{2000 \text{ km s}^{-1}} \right)^{-1} \left( \frac{y_{\text{br}}}{5} \right) \left( 1 - \frac{\alpha}{y_{\text{br}}} \right)^{-b} \\ &\quad \times [\xi F_\gamma^2 F_p \Gamma_s^2 \beta_s^2]_{y=y_{\text{br}}}. \end{aligned} \quad (36)$$

Similarly, from equation (25), we can obtain the temperature of the radiation measured in a rest frame

$$\begin{aligned} T_{\text{br}} &\equiv [\gamma_2 T_2]_{r=R_{\text{br}}} \\ &\approx \left( \frac{3\Psi c^2}{4\pi a R_\star^3} \right)^{1/4} [F_\gamma F_p^{1/4} \Gamma_s^{3/2} \beta_s^{1/2}]_{y=y_{\text{br}}} \\ &\quad \times y_{\text{br}}^{-1/2} \left( 1 - \frac{\alpha}{y_{\text{br}}} \right)^{-b/4} \\ &\approx 0.800 \times 10^6 \text{ K} \left( \frac{\dot{M}}{5 \times 10^{-5} M_\odot \text{ yr}^{-1}} \right)^{0.25} \\ &\quad \times \left( \frac{R_\star}{3R_\odot} \right)^{-0.5} \left( \frac{v_\infty}{2000 \text{ km s}^{-1}} \right)^{-0.25} \left( \frac{y_{\text{br}}}{5} \right)^{-0.5} \\ &\quad \times \left( 1 - \frac{\alpha}{y_{\text{br}}} \right)^{-b/4} [F_\gamma F_p^{1/4} \Gamma_s^{3/2} \beta_s^{1/2}]_{y=y_{\text{br}}}. \end{aligned} \quad (37)$$

The time-duration for the event arising from shock breakout can be estimated by

$$\begin{aligned} t_{\text{br}} &\approx \frac{R_{\text{ph}} - R_{\text{br}}}{v_{s,\text{br}}} = \frac{R_\star}{\beta_{s,\text{br}} c} (y_{\text{ph}} - y_{\text{br}}) \\ &\approx 6.96 \text{ s} \left( \frac{R_\star}{3R_\odot} \right) \beta_{s,\text{br}}^{-1} (y_{\text{ph}} - y_{\text{br}}), \end{aligned} \quad (38)$$

where  $v_{s,\text{br}} = \beta_{s,\text{br}} c \equiv v_s(r = R_{\text{br}})$  is the speed of the shock front at breakout.

## 6 RESULTS

Unlike the cases of non-relativistic and ultra-relativistic shocks, where the quantities characterizing the transient event from the shock breakout can be expressed with factorized scaling relations of input parameters (e.g., the eqs. 36-38 of Matzner & McKee 1999), for the trans-relativistic case here we must numerically solve the relevant equations for the characteristic quantities.

All the relevant equations are in Sec. 5, supplemented by the formulae for the wind mass function  $\Psi$ , the optical depth, and the surface mass density in Sec. 2 (and Appendix A when  $b = 1$ ). We can eliminate  $\dot{M}$  and  $v_\infty$  from the equations by substituting

$$\Psi = 4\pi \Sigma R_\star^2 y_{\text{ph}}, \quad (39)$$

where the surface mass density  $\Sigma$  is a function of  $\kappa$ ,  $\alpha$ , and  $b$  (eqs. 10 and 11). Since  $\alpha$  is a function of  $\varepsilon$  and  $b$  (eq. 6), we can then choose the input parameters to be  $E_{\text{in}}$ ,  $M_{\text{ej}}$ ,  $R_\star$ ,  $\varepsilon$ ,  $b$ , and  $\kappa$ .

Compared to the case of shock breakout from a star without a wind (Matzner & McKee 1999), here we have two additional parameters:  $\varepsilon$  and  $b$ , both describing the shape of the wind velocity profile (eqs. 5 and 6). However, in the case of a star, the opacity  $\kappa$  is fairly well determined so there are essentially only three parameters: the explosion energy  $E_{\text{in}}$ , the ejected mass  $M_{\text{ej}}$ , and the stellar radius  $R_\star$ . Although there is yet another parameter  $\zeta \equiv \rho_1/\rho_\star$  (see Appendix B) where  $\rho_\star \equiv M_{\text{ej}}/R_\star^3$ , which is typically 0.2 for blue supergiants and 0.5 for red supergiants (Calzavara & Matzner 2004), the characteristic quantities (at least the energy, the

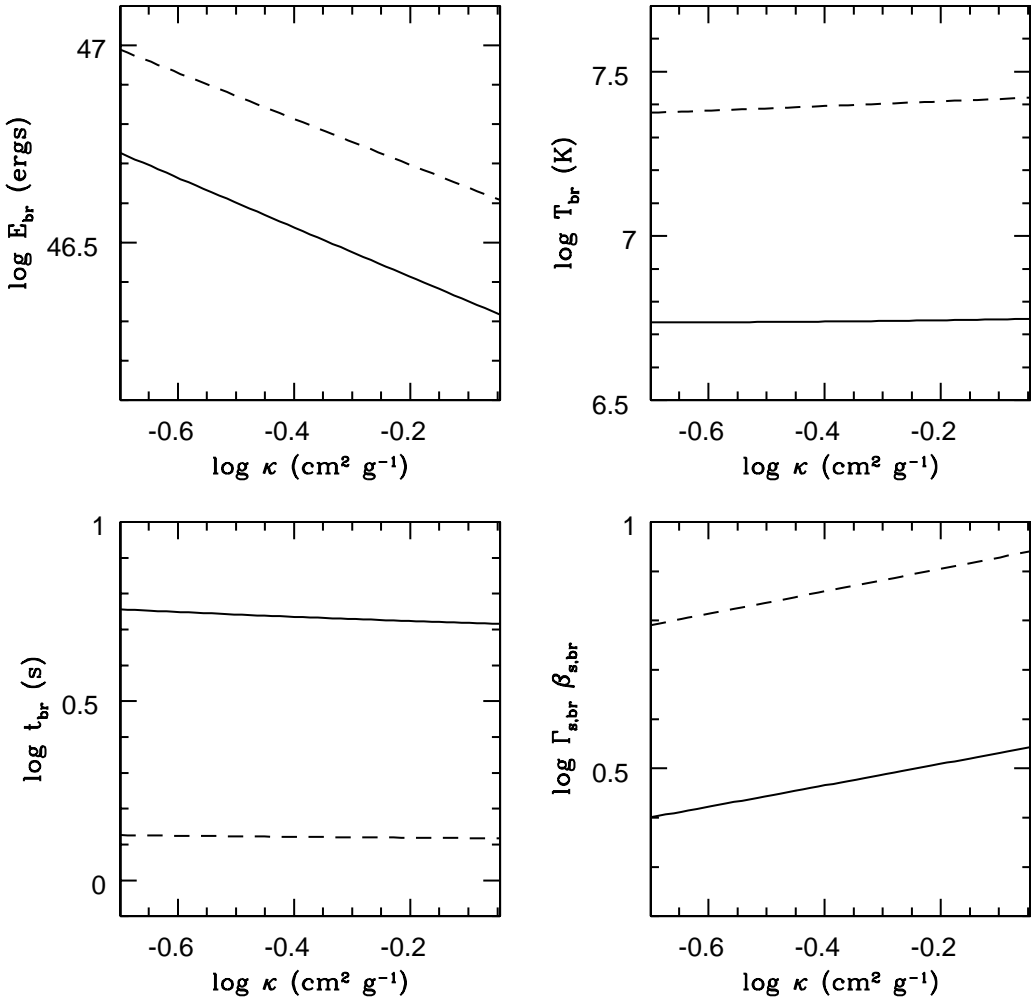


**Figure 4.** Characteristic quantities of shock emergence as functions of the opacity in the stellar wind. The solid line corresponds to  $\varepsilon = 10^{-2}$ . The dashed line corresponds to  $\varepsilon = 10^{-3}$ . Other parameters are:  $b = 5$ ,  $E_{\text{in}} = 10^{52}$  ergs,  $M_{\text{ej}} = 10M_{\odot}$ , and  $R_{\star} = 3R_{\odot}$ .

temperature, and the shock momentum) at shock breakout are extremely insensitive to  $\zeta$  (Matzner & McKee 1999). While for the problem here, i.e., a dense stellar wind surrounding a star, the opacity  $\kappa$  is poorly known. Modeling of the WR winds indicates that the opacity is in the range of  $0.3 - 0.9 \text{ cm}^2 \text{ g}^{-1}$  at sonic point, and somewhat greater at larger radii (Nugis & Lamers 2002).

The parameter  $\varepsilon$ , which is the ratio of the wind velocity at the stellar surface to the terminal velocity of the wind, is usually thought to be in the range of  $0.001 - 0.1$ , and typically around 0.01 (Schaerer 1996).

The parameter  $b$ , which characterizes the slope of the wind velocity in the region near the stellar surface, is taken to be unity in the standard model of stellar winds. However, as already mentioned in Sec. 2, for the winds of WR stars  $b$  can be much larger as argued by Robert (1994), Schmutz (1997), and Lépine & Moffat (1999), and is typically in the range of 4 – 6 (Nugis & Lamers 2002).

In our numerical modeling, we allow  $\kappa$  to vary from 0.2 to  $0.9 \text{ cm}^2 \text{ g}^{-1}$ ,  $\varepsilon$  to vary from  $10^{-5}$  to  $10^{-1}$ , and  $b$  from 1 to 10. We allow  $E_{\text{in}}$  to vary from  $10^{51}$  ergs (for normal core-collapse supernovae) to  $10^{53}$  ergs (for hypernovae),  $M_{\text{ej}}$  to vary from  $1M_{\odot}$  to  $20M_{\odot}$ . Although WR stars are compact,

to fully explore the effect of variation in the stellar radius on the results, we allow  $R_{\star}$  to vary from  $1R_{\odot}$  to  $30R_{\odot}$ . Whenever numbers are quoted, we refer to the fiducial values  $\kappa = 0.7 \text{ cm}^2 \text{ g}^{-1}$ ,  $\varepsilon = 0.01$ ,  $b = 5$ ,  $E_{\text{in}} = 10^{52}$  ergs,  $M_{\text{ej}} = 10M_{\odot}$ , and  $R_{\star} = 3R_{\odot}$ , unless otherwise stated.

Our numerical results for the characteristic quantities of the shock breakout, including the total energy ( $E_{\text{br}}$ , eq. 36), temperature ( $T_{\text{br}}$ , eq. 37), time-duration ( $t_{\text{br}}$ , eq. 38), and shock momentum ( $\Gamma_{s,\text{br}}\beta_{s,\text{br}}$ , eqs. 33, 34) are presented in Figs. 4–8.

Figure 4 shows  $E_{\text{br}}$ ,  $T_{\text{br}}$ ,  $t_{\text{br}}$ , and  $\Gamma_{s,\text{br}}\beta_{s,\text{br}}$  as functions of the opacity  $\kappa$ . Solid lines correspond to  $\varepsilon = 10^{-2}$ . Dashed lines correspond to  $\varepsilon = 10^{-3}$ . Other parameters take the fiducial values, as indicated in the figure caption. The breakout energy  $E_{\text{br}}$  decreases as the opacity increases. As  $\kappa$  increases from 0.2 to  $0.9 \text{ cm}^2 \text{ g}^{-1}$ ,  $E_{\text{br}}$  is reduced by a factor  $\approx 2.6$  when  $\varepsilon = 10^{-2}$ , and  $\approx 2.4$  when  $\varepsilon = 10^{-3}$ . The temperature and the breakout time are insensitive to the change in  $\kappa$ . The momentum of the shock front at the breakout time increases with the opacity. As  $\kappa$  increases from 0.2 to  $0.9 \text{ cm}^2 \text{ g}^{-1}$ ,  $\Gamma_{s,\text{br}}\beta_{s,\text{br}}$  increases by a factor  $\approx 1.4$  (for both  $\varepsilon = 10^{-2}$  and  $\varepsilon = 10^{-3}$ ). Similar to the case of breakout from a star, the results do not change dramatically with

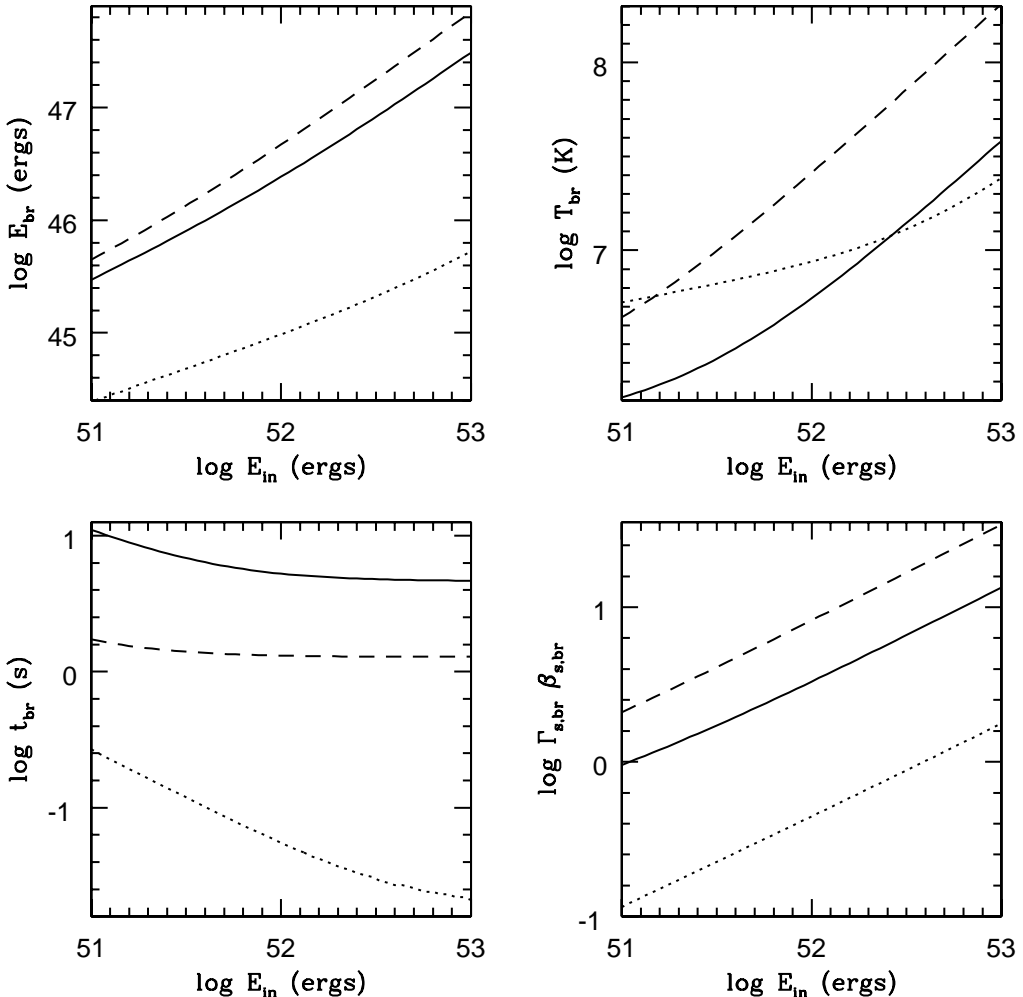


**Figure 5.** Characteristic quantities of shock emergence as functions of the explosion kinetic energy. The solid line corresponds to  $\varepsilon = 10^{-2}$ . The dashed line corresponds to  $\varepsilon = 10^{-3}$ . Other parameters are:  $b = 5$ ,  $\kappa = 0.7 \text{ cm}^2 \text{ g}^{-1}$ ,  $M_{\text{ej}} = 10M_{\odot}$ , and  $R_{\star} = 3R_{\odot}$ . The dotted line shows the solution for shock breakout from a star without a wind, with the same  $M_{\text{ej}}$ ,  $R_{\star}$ , and  $\kappa = 0.2 \text{ cm}^2 \text{ g}^{-1}$ ,  $\zeta = 1$ .

the opacity. Thus, the poor knowledge in the opacity in the stellar winds will not affect our results drastically.

All the dependence on  $\kappa$  manifests itself through the surface mass density in equation (11) (and eq. A4 when  $b = 1$ ), which shows that  $\Sigma \propto \kappa^{-1}$ . Since  $\Psi \propto \Sigma$ , we also have  $\Psi \propto \kappa^{-1}$ . Then, from the condition for the shock breakout (eq. 31), it can be derived that  $y_{\text{br}}$  increases with  $\kappa$ . From the dependence of  $E_{\text{br}}$ ,  $T_{\text{br}}$ ,  $t_{\text{br}}$ , and  $\Gamma_{s,\text{br}}\beta_{s,\text{br}}$  on  $\Psi$  and  $y_{\text{br}}$ , it is not hard to understand the trend shown in Fig. 4.

Figure 5 shows the same set of characteristic quantities as functions of the explosion kinetic energy. Symbols and values of parameters are similar to Fig. 4 and are explained in the figure caption. To compare with the results for a star without a wind, we show with dotted lines the corresponding characteristic quantities calculated for the shock breakout from a star with the corresponding formulae in Appendix B, for the same values of  $M_{\text{ej}}$  and  $R_{\star}$ , and  $\kappa = 0.2 \text{ cm}^2 \text{ g}^{-1}$ ,  $\zeta = 1$ .

As the explosion energy increases from  $10^{51}$  ergs to  $10^{53}$  ergs, the breakout energy increases by a factor  $\approx 104$  when  $\varepsilon = 10^{-2}$ , and  $\approx 157$  when  $\varepsilon = 10^{-3}$ . This increasing rate is much faster than that in the case of breakout from a star, in

which the breakout energy increases only by a factor of  $\approx 22$ . The increase in the temperature is also faster, which is by a factor of  $\approx 23$  when  $\varepsilon = 10^{-2}$ , and  $\approx 47$  when  $\varepsilon = 10^{-3}$  for a star with a dense wind, and only  $\approx 4.6$  for a star without a wind. While for the breakout time-duration, it appears that for the case of a stellar wind the time-duration does not change rapidly when  $E_{\text{in}}$  increases, in contrast to the case of a star. This is caused by the fact that a dense stellar wind has more room for the shock to accelerate than a star, so that the shock front is more relativistic (see the panel for the shock momentum) and its velocity is close to the speed of light. In Sec. 5 we have seen that, as the shock velocity approaches the speed of light, the breakout radius approaches  $y_{\text{max}}$  and the distance between  $y_{\text{max}}$  and  $y_{\text{ph}}$  does not change with the explosion energy.

The momentum of the shock front varies with  $E_{\text{in}}$  at about the same rate for the case of a stellar wind and the case of a star.

The curvature of the curves in Fig. 5 confirms our claim at the beginning of this section that in the trans-relativistic case the characteristic quantities of shock breakout in gen-

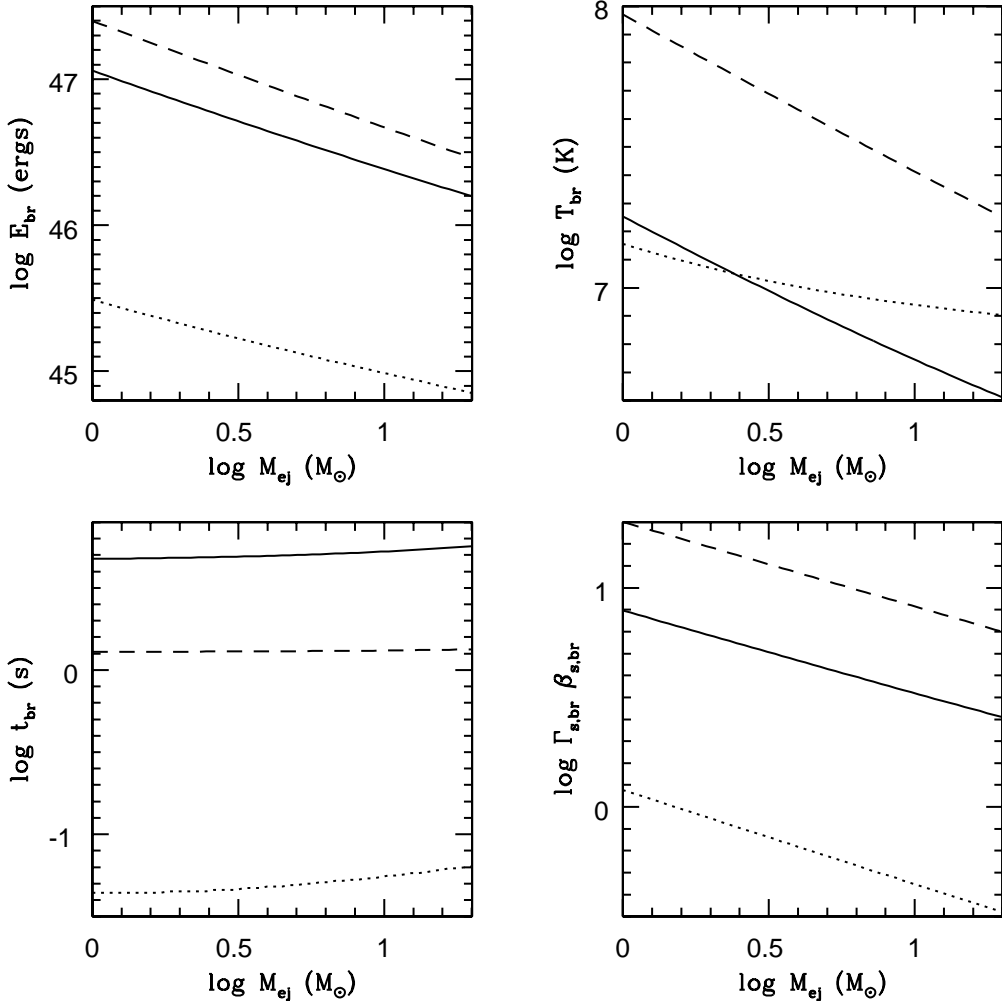


**Figure 6.** Characteristic quantities of shock emergence as functions of the ejected mass. The solid line corresponds to  $\varepsilon = 10^{-2}$ . The dashed line corresponds to  $\varepsilon = 10^{-3}$ . Other parameters are:  $b = 5$ ,  $\kappa = 0.7 \text{ cm}^2 \text{ g}^{-1}$ ,  $E_{\text{in}} = 10^{52} \text{ ergs}$ , and  $R_{\star} = 3R_{\odot}$ . The dotted line shows the solution for shock breakout from a star without a wind, with the same  $E_{\text{in}}$ ,  $R_{\star}$ , and  $\kappa = 0.2 \text{ cm}^2 \text{ g}^{-1}$ ,  $\zeta = 1$ .

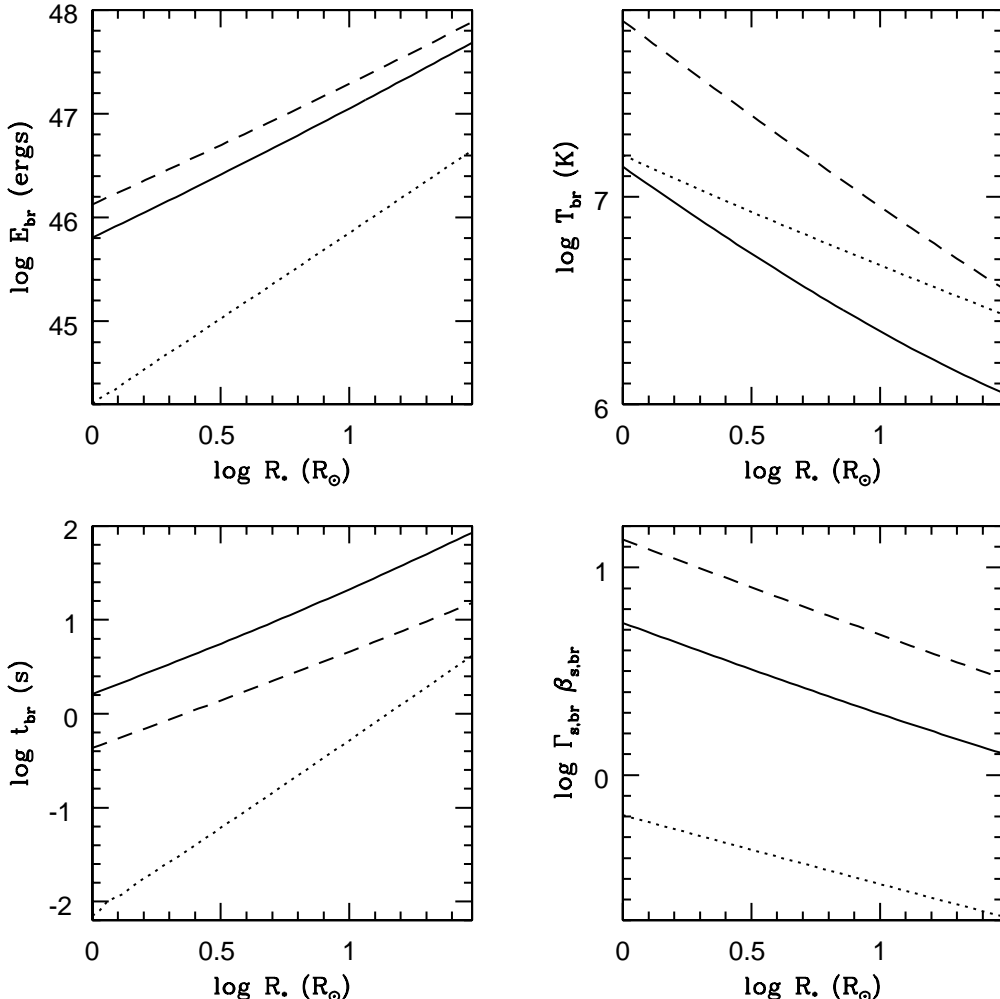
eral cannot be written as factorized scaling formulae of input parameters.

Figure 6 shows the characteristic quantities as functions of the ejected mass, with symbols and parameters similar to that in Fig. 5 (see the figure caption). As the ejected mass increases from  $1M_{\odot}$  to  $20M_{\odot}$ , the breakout energy decreases by a factor  $\approx 7.2$  when  $\varepsilon = 10^{-2}$ , and  $\approx 8.7$  when  $\varepsilon = 10^{-3}$ , faster than the case of a star for which the decreasing factor  $\approx 4.4$ . The temperature also drops faster. The variation in the breakout time-duration is not fast in both cases of stellar winds and stars. That is, the time-duration of the shock breakout is not very sensitive to the ejected mass. The momentum of the shock front drops slightly slower than that in the case of a star.

Figure 7 shows the characteristic quantities as functions of the core radius of the star, which, as in the case of a star (Matzner & McKee 1999), is the parameter that most dramatically affects the values of the characteristic quantities. As  $R_{\star}$  increases from  $1R_{\odot}$  to  $30R_{\odot}$ , the breakout energy increases by a factor  $\approx 76$  when  $\varepsilon = 10^{-2}$ , and  $\approx 57$  when  $\varepsilon = 10^{-3}$ . However, this is still somewhat smaller than that in the case of star without a wind, which is  $\approx 277$ . The tem-

perature drops very fast, caused by the rapid increase in the area of the surface emitting the radiation. As  $R_{\star}$  increases from  $1R_{\odot}$  to  $30R_{\odot}$ , the temperature drops by a factor of  $\approx 12$  when  $\varepsilon = 10^{-2}$ , and  $\approx 19$  when  $\varepsilon = 10^{-3}$ , in contrast to the factor  $\approx 5.8$  in the case of a star. The variation in the stellar radius also has dramatic effect on the breakout time-duration, although the effect is less prominent than in the case of a star. The factor by which the breakout time-duration increases is  $\approx 52$  when  $\varepsilon = 10^{-2}$ , and  $\approx 35$  when  $\varepsilon = 10^{-3}$ , in contrast to that  $\approx 590$  in the case of a star. The momentum of the shock front drops by a factor  $\approx 4.2$  when  $\varepsilon = 10^{-2}$ , and  $\approx 4.7$  when  $\varepsilon = 10^{-3}$ , similar to the factor  $\approx 3$  in the case of a star.

Finally, in Fig. 8 we show the characteristic quantities as functions of  $b$ . Interestingly, the breakout energy is not a monotonic function of  $b$ . When  $\varepsilon = 10^{-2}$ ,  $E_{\text{br}}$  minimizes at  $b \approx 2$ . The value of  $E_{\text{br}}$  at  $b = 5$  is smaller than that at  $b = 1$  by a factor  $\approx 1.3$ . When  $\varepsilon = 10^{-3}$ ,  $E_{\text{br}}$  minimizes at  $b \approx 1.4$ . The value of  $E_{\text{br}}$  at  $b = 5$  is larger than that at  $b = 1$  by a factor  $\approx 2$ . Overall, the change in  $E_{\text{br}}$  is not essential if  $b$  is in the range of  $4 - 6$ . The temperature monotonically increases with  $b$ , resulting from the fact the breakout radius decreases



**Figure 7.** Characteristic quantities of shock emergence as functions of the core radius of the star. The solid line corresponds to  $\varepsilon = 10^{-2}$ . The dashed line corresponds to  $\varepsilon = 10^{-3}$ . Other parameters are:  $b = 5$ ,  $\kappa = 0.7 \text{ cm}^2 \text{ g}^{-1}$ ,  $E_{\text{in}} = 10^{52} \text{ ergs}$ , and  $M_{\text{ej}} = 10M_{\odot}$ . The dotted line shows the solution for shock breakout from a star without a wind, with the same  $E_{\text{in}}$ ,  $M_{\text{ej}}$ , and  $\kappa = 0.2 \text{ cm}^2 \text{ g}^{-1}$ ,  $\zeta = 1$ .

as  $b$  increases. The breakout time-duration decreases with increasing  $b$ , but approaches a constant if  $b$  is very large. The momentum of the shock front increases with  $b$ , caused by the fact that a larger  $b$  results in a steeper density profile and more acceleration of the shock.

From Figs. 4–7, and Fig. 8 at  $b = 4–6$ , the effects of variation in  $\varepsilon$  from  $10^{-2}$  to  $10^{-3}$  can be summarized as follows: the breakout energy  $E_{\text{br}}$  increases by a factor of  $1.6–2$ ; the temperature  $T_{\text{br}}$  increases by a factor of  $3–5$ ; the shock momentum  $\Gamma_{s,\text{br}}\beta_{s,\text{br}}$  increases by a factor of  $2.3–2.5$ ; and the time-duration  $t_{\text{br}}$  decreases by a factor of  $3.5–6$ .

Figures 5–7 also show that, for a star with a dense wind the shock breakout is more energetic than that for a star without a wind. This is mainly caused by the fact that a dense wind effectively increases the radius of a star so that the shock has more room and more time for acceleration. For the same set of common parameters ( $E_{\text{in}}$ ,  $M_{\text{ej}}$ ,  $R_{\star}$ , but not  $\kappa$ ), for typical parameters the total energy of the radiation from shock breakout is larger by a factor more than 10 if the star is surrounded by a dense wind. The momentum of the shock front is also increased by a factor  $\sim 10$ . The temperature does not show a universal trend, but is broadly

similar in the two cases. This is because of the fact that the inclusion of a dense stellar wind prompts the total energy released by shock breakout but in the meantime it also increases the effective radius of the star. The time-duration is larger for the case of stellar winds as a result of increase in the effective radius of the star.

The shock breakout occurs inside the maximum acceleration radius  $R_a = (1+b)\alpha R_{\star}$  in all the models presented in Figs. 4–8, except the model of  $\varepsilon = 10^{-2}$  in Fig. 8 where the shock breakout occurs at a radius larger than  $R_a$  when  $b < 1.23$ .

In the above calculations of the breakout time-duration, the light-travel-time has not been taken into account. In other words,  $t_{\text{br}}$  is the duration measured in the SN frame. The duration observed by a remote observer,  $t_{\text{br,obs}}$ , differs from  $t_{\text{br}}$  by an effect caused by the travel-time of lights—which arises from the fact that an observer will see more distant annuli of the stellar disk with a time-delay (Enzman & Burrows 1992). The effect of light-travel-time is extremely important when the  $t_{\text{br}}$  calculated by equation (38) is short, which is definitely true here since WR stars are compact. Thus, approximately, the observed dura-

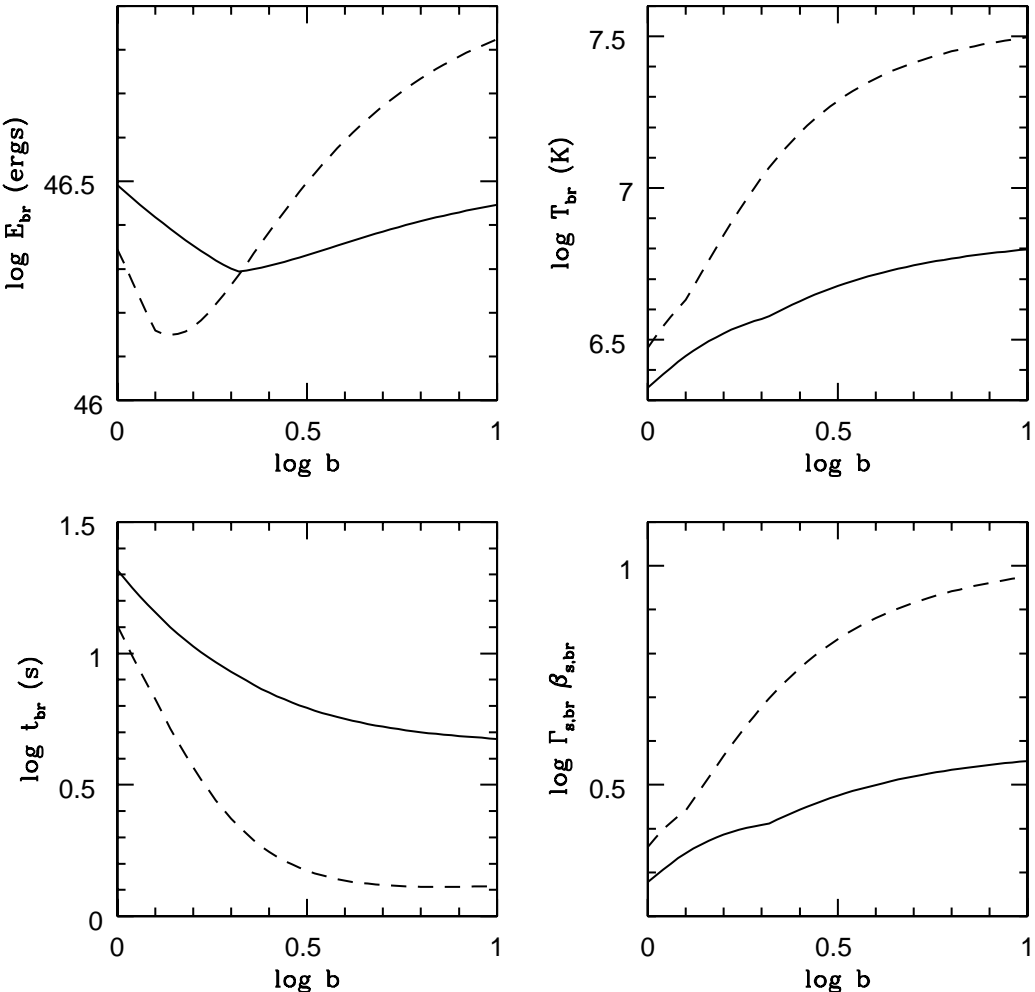


**Figure 8.** Characteristic quantities of shock emergence as functions of the wind parameter  $b$ . The solid line corresponds to  $\varepsilon = 10^{-2}$ . The dashed line corresponds to  $\varepsilon = 10^{-3}$ . Other parameters are:  $b = 5$ ,  $\kappa = 0.7 \text{ cm}^2 \text{ g}^{-1}$ ,  $E_{\text{in}} = 10^{52} \text{ ergs}$ ,  $M_{\text{ej}} = 10M_{\odot}$ , and  $R_{\star} = 3R_{\odot}$ .

tion of the shock breakout is given by

$$t_{\text{br,obs}} = \max \left( t_{\text{br}}, \frac{R_{\text{ph}}}{c} \right), \quad (40)$$

where  $R_{\text{ph}}$  is the photospheric radius of the star.

For all the models presented in Figs. 4–8 the light-travel-time is much larger than  $t_{\text{br}}$ , so the observed duration is given by  $R_{\text{ph}}/c$ . Note,  $R_{\text{ph}} = y_{\text{ph}}R_{\star}$ , and  $y_{\text{ph}}$  is a function of  $\varepsilon$  and  $b$ . For the models in Figs. 4–6,  $b = 5$  and  $R_{\star} = 3R_{\odot}$ , therefore  $t_{\text{br,obs}} = 22.4 \text{ s}$  when  $\varepsilon = 10^{-2}$ , and  $t_{\text{br,obs}} = 12.2 \text{ s}$  when  $\varepsilon = 10^{-3}$ .

For the models in Figs. 7 and 8 where  $R_{\star}$  and  $b$  vary, we plot the value  $t_{\text{br,obs}} = R_{\text{ph}}/c$  in Fig. 9. All the values of  $R_{\text{ph}}/c$  are larger than the corresponding values of  $t_{\text{br}}$  in Figs. 7 and 8 (hence we wrote  $t_{\text{br,obs}} = R_{\text{ph}}/c$ ), as can be seen by comparing the figures.

Numerical results for a set of SN models are presented in Table 1.

## 7 APPLICATION TO GRB 060218/SN 2006AJ

As stated in the Introduction, recently it was claimed that supernova shock breakout has been observed in the early

X-ray afterglow of GRB 060218, based on the observation that a fraction ( $\approx 20\%$ ) of the radiation in the early lightcurve (from 159 s up to  $\sim 10,000$  s after the trigger of the burst) is a soft black-body of temperature  $\sim 0.17 \text{ keV}$  (Campana et al. 2006). The total energy estimated for this black-body component is  $\sim 10^{49} \text{ ergs}$  in the  $0.3 - 10 \text{ keV}$  band. A reanalysis carried out by Butler (2006) revealed an even larger energy in the black-body, which is  $\sim 2 \times 10^{50} \text{ ergs}$ , lasting  $\sim 300 \text{ s}$ . According to Butler (2006), the black-body component even dominates the X-ray lightcurve after about 1,000 s from the trigger.

The overall constraint on the black-body component in the early X-ray afterglow of GRB 060218 is thus as follows: total energy  $\gtrsim 10^{49} \text{ ergs}$ , temperature in the range of  $0.1 - 0.19 \text{ keV}$  (i.e.,  $1.2 - 2.2 \times 10^6 \text{ K}$ ), and duration  $\gtrsim 300 \text{ s}$  (Campana et al. 2006; Butler 2006).

In this section, we apply the procedure developed in previous sections to calculate the characteristic quantities of the shock breakout event for SN 2006aj with the assumption that the supernova was produced by the core-collapse of a WR star surrounded by a dense wind, and examine if the black-body component in GRB 060218 can be attributed to the supernova shock breakout.

**Table 1.** Models of supernova explosion and predicted characteristic parameters of shock breakout. Input parameters are:  $E_{\text{in}}$ , explosion kinetic energy;  $M_{\text{ej}}$ , ejected mass;  $R_{\star}$ , core radius of the progenitor (the radius at optical depth of 20);  $\kappa$ , opacity in the wind;  $\varepsilon$ , ratio of the wind velocity at the stellar surface ( $r = R_{\star}$ ) to the terminal velocity of the wind (eq. 6);  $b$ , specifying the profile of the wind velocity (eq. 5). Output parameters are:  $E_{\text{br}}$ , total energy of the radiation from shock breakout;  $T_{\text{br}}$ , temperature of the radiation from shock breakout;  $t_{\text{br,obs}}$ , observed time-duration of the shock breakout event. Models 1–4 are normal SNe Ibc. Models 5 and 6 are hypernovae. In all cases,  $t_{\text{br,obs}}$  is determined by the light-travel-time  $R_{\text{ph}}/c$ , where  $R_{\text{ph}}$  is the photospheric radius of the progenitor.

Model	$E_{\text{in}}$ ( $10^{51}$ ergs)	$M_{\text{ej}}$ ( $M_{\odot}$ )	$R_{\star}$ ( $R_{\odot}$ )	$\kappa$ ( $\text{cm}^2 \text{ g}^{-1}$ )	$\varepsilon$	$b$	$E_{\text{br}}$ ( $10^{46}$ ergs)	$T_{\text{br}}$ ( $10^6$ K)	$t_{\text{br,obs}}$ (sec)
1	1	3	3	0.7	0.01	5	0.56	2.2	22
2	1	4	3	0.2	0.02	5	1.2	1.9	30
3	1.5	6	5	0.5	0.01	1	1.4	1.0	86
4	2	2	5	0.7	0.001	5	4.5	10	20
5	40	10	3	0.2	0.01	5	22	16	22
6	60	15	5	0.7	0.001	6	56	68	20

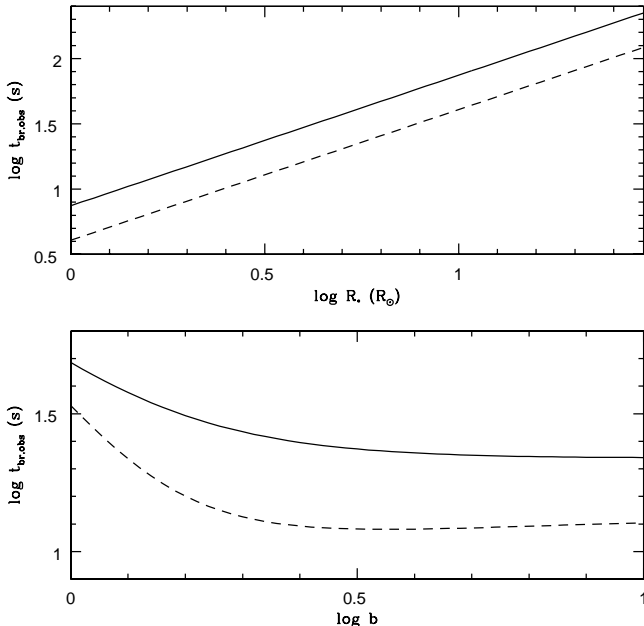


**Figure 9.** The observed time-duration of shock breakout (defined by eq. 40) for the models in Figs. 7 (upper panel) and 8 (lower panel), versus the stellar radius and the parameter  $b$ , respectively. In all cases  $R_{\text{ph}}/c > t_{\text{br}}$  so  $t_{\text{br,obs}} = R_{\text{ph}}/c$ . The solid line corresponds to  $\varepsilon = 10^{-2}$ . The dashed line corresponds to  $\varepsilon = 10^{-3}$ .

First, we apply the procedure to the WR stars in Fig. 1, which are among the best studied catalog of WR stars with model-determined stellar and photospheric radii (Hamann, Koesterke & Wessolowski 1995; Koesterke & Hamann 1995; Gräfener et al. 1998). We pick up only stars with  $y_{\text{ph}} = R_{\text{ph}}/R_{\star} > 2$ , since otherwise the  $\varepsilon$  given by our simplified model would be too small (Fig. 3). The sub-sample so selected consists of total 36 stars, including 20 Galactic WCs, 10 Galactic WNs, and 6 LMC WCs. The majority of WC stars have been included. Since these stars were modeled by the standard stellar wind model, we choose  $b = 1$ . The  $\alpha$  parameter is then obtained from the published values of  $y_{\text{ph}}$  in the papers cited above by equations (A2) and (A3). The value of  $\varepsilon$  is calculated with equation (6). Then, with the published values of  $\dot{M}$ ,  $v_{\infty}$ ,

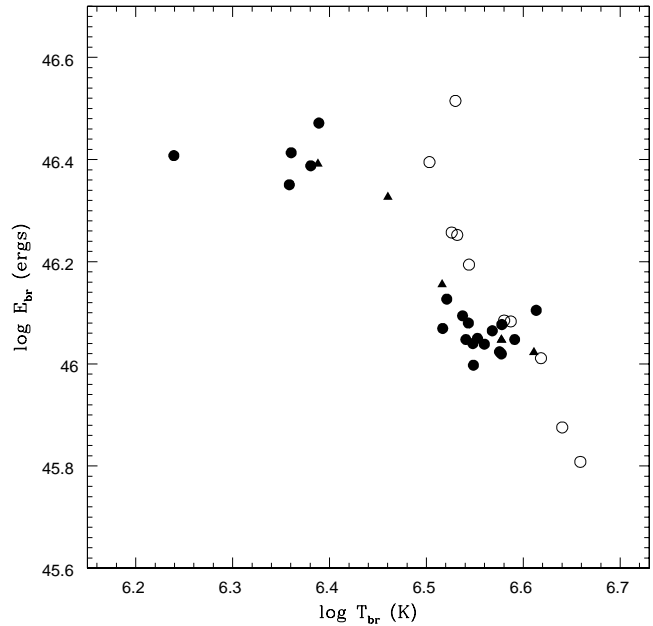


**Figure 10.** Energy versus temperature of shock breakout in Type Ibc supernovae produced by core-collapse of a sample of WR stars with  $R_{\text{ph}}/R_{\star} > 2$ .

$R_{\star}$ , and  $R_{\text{ph}}$ , the constant mean opacity  $\kappa$  can be calculated with equation (A4).

For the explosion energy and the ejected mass, we take the values obtained from modeling the lightcurve of SN 2006aj:  $E_{\text{in}} = 2 \times 10^{51}$  ergs,  $M_{\text{ej}} = 2M_{\odot}$  (Mazzali et al. 2006). Then, for each star we have all of the six parameters needed for calculating the characteristic quantities of shock breakout.

Our results are shown in Fig. 10 for the breakout energy versus the breakout temperature, and in Fig. 11 for the breakout shock momentum versus the breakout time-duration. Note, here the breakout duration has taken into account the light-travel-time (eq. 40), so corresponds to the observed time-duration. From Fig. 10 we see that, although the temperature is in the range of the black-body component in the afterglow of GRB 060218 for several WC stars (on the left end), the total energy of the radiation arising from the

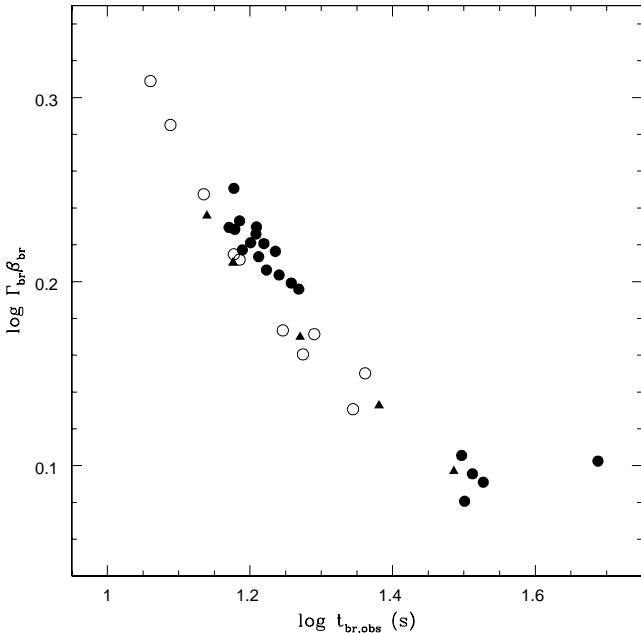


**Figure 11.** Shock momentum versus the observed time-duration of shock breakout in Type Ibc supernovae produced by core-collapse of the same sample of WRs in Fig. 10.

shock breakout never exceeds  $10^{47}$  ergs, i.e., always smaller than the total energy of the observed black-body component in GRB 060218 by more than two orders of magnitude.

From Fig. 11, the time-duration of the shock breakout never exceeds 100 s, also well below the observational limit of the black-body component in GRB 060218.

Thus, it appears that none of the stars in the considered sample of WRs is able to produce a supernova with shock breakout energy that is large enough to explain the black-body component observed in the early X-ray afterglow of GRB 060218.

Of course, GRBs are rare events compared to supernovae (Podsiadlowski et al. 2004), they may require progenitors that are in more extreme conditions than the WRs in our sample. To test the possibility for explaining the black-body component in GRB 060218 with shock breakout from WR stars in a larger parameter space, we plot the breakout energy and the temperature, calculated with our model, against the stellar core radius—the parameter that the characteristic quantities of the shock breakout are most sensitive to—in Fig. 12 and Fig. 13, for  $b = 5$ ,  $\kappa = 0.2 \text{ cm}^2 \text{ g}^{-1}$  (a smaller value of  $\kappa$  is chosen to increase the breakout energy),  $E_{\text{in}} = 2 \times 10^{51}$  ergs,  $M_{\text{ej}} = 2M_{\odot}$  (constrained by modeling the lightcurve of SN 2006aj), and  $\varepsilon$  varying from  $10^{-2}$  to  $10^{-5}$ . The lower limit for the energy of the black-body component in GRB 060218 is shown in Fig. 12 by the horizontal dashed line. Note, this contains only the energy in 0.3–10 keV. The bolometric energy should be larger by a factor  $\approx 1.2$  (using a black-body temperature = 0.17 keV). The range of the black-body temperature is bounded by the two horizontal dashed lines in Fig. 13.

The upper limit on the stellar core radius is chosen to be  $100R_{\odot}$ , which is more than enough for WR stars. Then, from Fig. 12, to get a breakout energy  $\gtrsim 10^{49}$  ergs, the radius of the star must be  $\gtrsim 25R_{\odot}$ , and in addition, the parameter

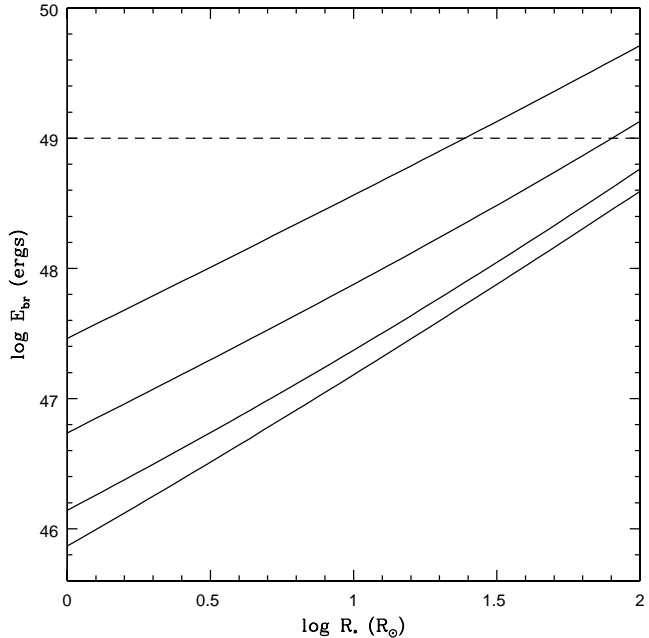


**Figure 12.** Breakout energy as a function of the radius of the star. Solid lines correspond to  $\varepsilon = 10^{-2}$ ,  $10^{-3}$ ,  $10^{-4}$  and  $10^{-5}$  (upward). Other parameters are:  $b = 5$ ,  $\kappa = 0.2 \text{ cm}^2 \text{ g}^{-1}$ ,  $E_{\text{in}} = 2 \times 10^{51}$  ergs, and  $M_{\text{ej}} = 2M_{\odot}$ . The dashed line represents the lower limit in the total energy of the black-body component in the X-ray afterglow of GRB 060218.

$\varepsilon$  must be  $< 10^{-4}$  if  $R_{*} < 80R_{\odot}$ . To get a temperature in the range of  $1.2 - 2.2 \times 10^6$  K, from Fig. 13,  $\varepsilon$  must satisfy  $\varepsilon > 10^{-4}$  if  $R_{*} < 80R_{\odot}$ . These conflict conditions on  $\varepsilon$  imply that it is impossible to interpret the black-body component in the early X-ray afterglow of GRB 060218 by SN shock breakout from a progenitor WR star with a core radius  $< 80R_{\odot}$ . Although it is possible to satisfy both the energy and the temperature constraints if the progenitor star has a core radius  $> 80R_{\odot}$ , it is very unlikely that there exists WR stars having so large stellar radii.

## 8 SUMMARY, CONCLUSION, AND DISCUSSIONS

We have presented a simple model for calculating the characteristic quantities (total energy, temperature, time-duration, and shock momentum) for the flashes arising from shock breakout in Type Ibc supernovae formed from the core-collapse of Wolf-Rayet stars surrounded by dense stellar winds. The wind velocity is modeled by equation (5), a profile that is often adopted in the study of stellar winds. However, in contrast to the case for O-stars where the parameter  $b$  is close to unity, for WR star winds  $b$  can be much larger and is usually in the range of 4–6 (Nugis & Lamers 2002). The opacity of the wind is assumed to be a constant, which is a major simplification in our model but allows us to solve the problem semi-analytically. Modeling of the opacity in the winds of WR stars indicates that  $\kappa$  is in the range of  $0.3 - 0.9 \text{ cm}^2 \text{ g}^{-1}$  (Nugis & Lamers 2002).

Our model is an extension of the existing model for calculating the characteristic quantities for SN shock break-

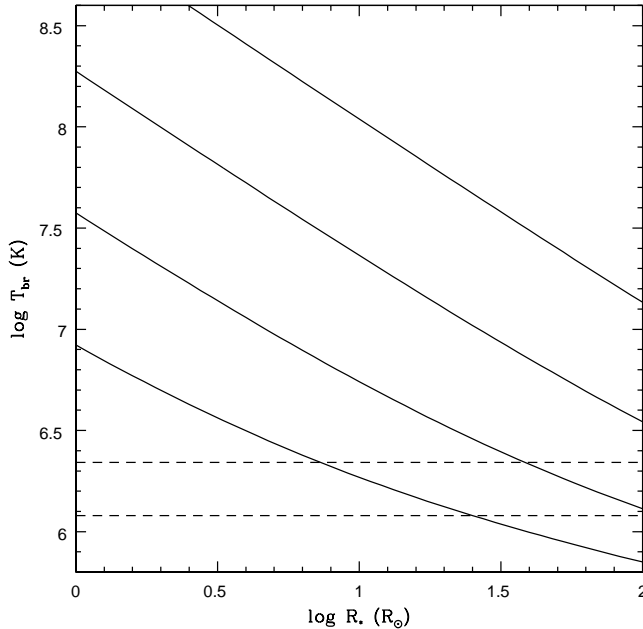


**Figure 13.** Same as Fig. 12 but for the breakout temperature. The two dashed lines bound the range of the temperature of the black-body component in the X-ray afterglow of GRB 060218.

out from a star without a wind, which is suitable for Type II SNe (Imshennik & Nadézhin 1988, 1989; Matzner & McKee 1999; Tan, Matzner & McKee 2001). Due to the compactness of WR stars, the shock momentum is expected to be trans-relativistic at the time of breakout. Thus, we have followed Blandford & McKee (1976), Gnatyk (1985), and Tan, Matzner & McKee (2001) to take into account the relativistic effects.

Due to the large optical depth in the wind, the SN shock breakout occurs in the wind region rather than inside the star. This is equivalent to say that the presence of a dense stellar wind effectively increases the radius of the star. As a result, the shock has more room and more time for acceleration, and the shock breakout appears to be more energetic than in the case for the same star but the effect of the stellar winds is not taken into account (see, e.g., Blinnikov et al. 2002).

The formulae for determining the radius where the shock breakout occurs and for computing the characteristic quantities for the radiation arising from shock breakout are collected in Sec. 5. They include equations (31), determining the breakout radius; (33) and (34), evaluating the momentum of the shock; (36), (37), and (38), calculating the energy, temperature, and the time-duration of the radiation from shock breakout. Although exact and analytic solutions are impossible caused by the trans-relativistic nature of the problem, all the equations are algebraic so a simple numerical program is able to calculate all the characteristic quantities. The model contains six input parameters: the explosion kinetic energy ( $E_{\text{in}}$ ), the ejected mass ( $M_{\text{ej}}$ ), the core radius of the star ( $R_{\star}$ , the radius where the optical depth is equal to 20), the opacity in the wind ( $\kappa$ ), the parameter  $b$  specifying the wind velocity profile, and the ratio of the wind velocity at the stellar surface ( $r = R_{\star}$ ) to the terminal velocity of the wind ( $\varepsilon$ ).

Our numerical results are summarized in Figs. 4–8 and Table 1. Figs. 4–8 illustrate how the characteristic quantities vary with the input parameters. As in the case of shock breakout from a star without a wind, the core radius of the star is the most important parameter affecting the results. That is, the characteristic quantities are most sensitive to the variation in the stellar radius. This feature leads to the possibility for distinguishing the progenitors of SNe by observing the transient events from the shock breakout (Calzavara & Matzner 2004). In addition, in the case of dense stellar winds the results are more sensitive to the variation in the SN explosion kinetic energy. For example, roughly speaking,  $E_{\text{br}} \propto E_{\text{in}}$  when the star has a dense wind, in contrast to  $E_{\text{br}} \propto E_{\text{in}}^{0.6}$  in the case of a star without a wind. Overall, the shock breakout from a star with a dense wind is more energetic than that from a star without a wind. For a star of the same radius, and for the same explosion kinetic energy and ejected mass, the total energy released by the shock breakout is larger by a factor  $\gtrsim 10$  if the star is surrounded by a thick wind. The time-duration is also larger, and the shock momentum at the time of breakout is more relativistic.

For an explosion energy of  $10^{51}$  ergs and ejected mass of  $3M_{\odot}$  (typical values for normal SNe Ibc), we get a breakout energy  $E_{\text{br}} \approx 5.6 \times 10^{45}$  ergs and a temperature  $T_{\text{br}} \approx 2.2 \times 10^6$  K  $\approx 0.19$  keV if other parameters take fiducial values ( $R_{\star} = 3R_{\odot}$ ,  $\kappa = 0.7$  cm $^2$  g $^{-1}$ ,  $b = 5$ , and  $\varepsilon = 0.01$ ). For an explosion energy of  $5 \times 10^{52}$  ergs and ejected mass of  $10M_{\odot}$  (typical values for hypernovae), we get a breakout energy  $E_{\text{br}} \approx 1.4 \times 10^{47}$  ergs and a temperature  $T_{\text{br}} \approx 2.1 \times 10^7$  K  $\approx 1.8$  keV. The observed time-duration of the breakout, which is given by  $R_{\text{ph}}/c$  (Sec. 6), is  $\approx 22$  s in both cases. More numerical results are shown in Table 1.

We have applied our model to GRB 060218/SN 2006aj, in which a soft black-body component has been observed in the early X-ray afterglow of the GRB and interpreted as an evidence for the supernova shock breakout (Campana et al. 2006). We take the values of the SN explosion energy and the ejected mass obtained from modeling the lightcurve of the supernova (Mazzali et al. 2006). we find that, the energy released by the shock breakout in a thick wind of a WR progenitor star resulted from the supernova explosion is too small to explain the black-body radiation in GRB 060218, unless the progenitor WR star has an unrealistic large core radius  $> 80M_{\odot}$ . Thus, we conclude that the black-body component in the X-ray afterglow of GRB 060218 cannot be attributed to the shock breakout in the underlying supernova, it must originate from other processes which might be related to the GRB outflow (see, e.g., Fan, Piran & Xu 2006).

One may argue that GRB-connected SNe should be highly aspherical so that our spherical model might have under-estimated the energy of the shock breakout. Indeed, aspherical explosion has been claimed to be observed in the luminous Type Ic SN 2003jd, in which the double-lined profiles in the nebular lines of neutral oxygen and magnesium revealed in later-time observations by Subaru and Keck is explained as a result of observing an aspherical supernovae along a direction almost perpendicular to the axis of the explosion (Mazzali et al. 2005). However, for SN 2006aj, there is no any evidence for aspherical explosion. Modeling of the afterglow emission (Fan, Piran & Xu 2006), as well as obser-

vation on the radio afterglow (Soderberg et al. 2006), indicates that the outflow associated with GRB 060218 is mildly relativistic so should be more or less spherical.

We should also remark that whether the progenitors of GRBs are surrounded by dense winds is still an open question. Although a wind-type density profile is naturally expected for the environment surrounding a GRB as its progenitor is broadly thought to be a massive star, observations on the GRB afterglows have revealed that most of the afterglow data are consistent with a constant density external medium and only a handful of bursts can be well modeled by the wind model (Berger et al. 2003; Zhang & Mészáros 2004; Panaitescu 2005; Fryer, Rockefeller & Young 2006, and references therein). For the case of GRB 060218, modeling of its afterglow has ruled out a dense circum-burst wind profile (Fan, Piran & Xu 2006).

A theoretical argument against strong winds surrounding GRB progenitors comes from the consideration of angular momentum (Yoon & Langer 2005; Woosley & Heger 2006a, and references therein). For a black hole formed from the core-collapse of a massive star to have a disk rotating around it and to launch a relativistic jet, the progenitor star must rotate rapidly with the specific angular momentum in the core  $j \gtrsim 3 \times 10^{16} \text{ cm}^2 \text{ s}^{-1}$  (MacFadyen & Woosley 1999). To satisfy this requirement, the progenitor star should not have had a phase with an intense stellar wind since a dense wind is very effective in removing angular momentum. Given the fact that the mass-loss rate of a star sensitively depends on its metallicity (Vink & de Koter 2005) and the observations that GRBs prefer to occur in galaxies with low metallicity (Fynbo et al. 2003; Hjorth et al. 2003a; Le Floc'h et al. 2003; Sollerman et al. 2005; Fruchter et al. 2006; Stanek et al. 2006), it is reasonable to expect that the progenitors of GRBs should not have dense stellar winds surrounding them. Even in this situation, however, the radius of the massive progenitor star is also very unlikely to be large enough ( $> 80R_\odot$ ) to explain the black-body component in GRB 060218 since its progenitor star has only a mass  $\sim 20M_\odot$  as obtained by modeling the SN lightcurve (Mazzali et al. 2006). In addition, if the progenitor does not have a thick wind, then in calculating the results for the shock breakout one should use the formulae in Appendix B for a star without a wind. But in Sec. 6 we have seen that the formulae for a star without a wind give rise to smaller total energy in the radiation from the shock breakout than the formulae for a star with a dense wind.

Despite the disappointing result on GRB 060218/SN 2006aj, our model is expected to have important applications to Type Ibc supernovae since whose progenitors are broadly believed to be WR stars. In addition, some Type II supernovae appear also to be related to progenitor stars with intensive stellar winds, e.g. SN IIn (also called IIdw) (Hamuy 2004). Observations on the transient events from SN shock breakout will be the most powerful approach for diagnosing the progenitors of supernovae. For this goal we would like to mention *LOBSTER*, an upcoming space observatory dedicated to detect soft X-ray flashes from shock breakout in supernovae (Calzavara & Matzner 2004).

## ACKNOWLEDGMENTS

The author thanks Bohdan Paczyński for many inspiring discussions on gamma-ray bursts, supernovae, and shock breakout.

## REFERENCES

Berger E., Kulkarni S. R., Frail D. A., 2001, *ApJ*, 560, 652  
 Berger E., Soderberg A. M., Frail D. A., Kulkarni S. R., 2003, *ApJ*, 587, L5  
 Blandford R. D., McKee C. F., 1976, *Phys. Fluids*, 19, 1130  
 Blinnikov S. I., Eastman R., Bartunov O. S., Popolitov V. A., Woosley S. E., 1998, *ApJ*, 496, 454  
 Blinnikov S., Lundqvist P., Bartunov O., Nomoto K., Iwamoto K., 2000, *ApJ*, 532, 1132  
 Blinnikov S. I., Nadyozhin D. K., Woosley S. E., Sorokina E. I., 2002, in *Nuclear Astrophysics*, ed. W. Hillebrandt & E. Müller (Garching: Max-Planck-Institut für Astrophysik), p. 144  
 Bloom J. S., Djorgovski S. G., Kulkarni S. R., Frail D. A., 1998, *ApJ*, 507, L25  
 Bloom J. S. et al., 1999, *ApJ*, 518, L1  
 Butler N. R., 2006, *astro-ph/0604083*  
 Calzavara A. J., Matzner C. D., 2004, *MNRAS*, 351, 694  
 Campana S. et al., 2006, *astro-ph/0603279*  
 Chen H.-W., Prochaska J. X., Bloom J. S., 2006, *astro-ph/0602144*  
 Christensen L., Hjorth J., Gorosabel J., 2004, *A&A*, 425, 913  
 Cobb B. E., Bailyn C. D., van Dokkum P. G., Natarajan P., 2006, *astro-ph/0603832*  
 Colgate S. A., 1968, *Canadian J. Phys.*, 46, S476  
 Costa E. et al., 1997, *Nature*, 387, 783  
 Della Valle M., 2006, *astro-ph/0604110*  
 Enzman L., Burrows A., 1992, *ApJ*, 393, 742  
 Fan Y., Piran T., Xu D., 2006, *astro-ph/0604016*  
 Filippenko A. V., 2004, in *The Fate of the Most Massive Stars*, ed. R. Humphreys & K. Stanek (San Francisco: ASP), p. 34  
 Frail D. A., Kulkarni S. R., Nicastro S. R., Feroci M., Taylor G. B., 1997, *Nature*, 389, 261  
 Frail D. A. et al., 2002, *ApJ*, 565, 829  
 Fruchter A. S. et al., 1999a, *ApJ*, 516, 683  
 Fruchter A. S. et al., 1999b, *ApJ*, 519, L13  
 Fruchter A. S. et al., 2006, *astro-ph/0603537*  
 Fryer C. L., Rockefeller G., Young P. A., 2006, *astro-ph/0604432*  
 Fynbo J. P. U. et al., 2003, *A&A*, 406, L63  
 Galama T.J. et al., 1998, *Nature*, 395, 670  
 Gnatyk B. I., 1985, *Sov. Astron. Lett.*, 11, 331  
 Gräfener G., Hamann W.-R., 2005, *A&A*, 432, 633  
 Gräfener G., Hamann W.-R., Hillier D. J., Koesterke L., 1998, *A&A*, 329, 109  
 Hamann W.-R., Koesterke L., 2000, *A&A*, 360, 647  
 Hamann W.-R., Koesterke L., Wessolowski, 1995, *A&A*, 299, 151  
 Hammer F., Flores H., Schaefer D., Dessauges-Zavadsky M., Le Floc'h E., Puech M., 2006, *astro-ph/0604461*  
 Hamuy M., 2004, in *Stellar collapse*, ed. C. L. Fryer (Dordrecht: Kluwer Academic Publishers), p. 39

Hjorth J. et al., 2003a, ApJ, 597, 699  
 Hjorth J. et al., 2003b, Nature, 423, 847  
 Ignace R., Oskinova L. M., Foulon C., 2000, MNRAS, 318, 214  
 Imshennik V. S., Nadézhin D. K., 1988, Soviet Astron. Lett., 14, 449  
 Imshennik V. S., Nadézhin D. K., 1989, Ap. Space Phys. Rev., 8, 1  
 Iwamoto, K., et al. 1998, Nature, 395, 672  
 Klein R. I., Chevalier R. A., 1978, ApJ, 223, L109  
 Klose S. et al., 2004, ApJ, 128, 1942  
 Koesterke L., Hamann W.-R., 1995, A&A, 299, 503  
 Langer N., 1989, A&A, 210, 93  
 Le Floc'h E. et al., 2003, A&A, 400, 499  
 Lépine S., Moffat A. F. J., 1999, ApJ, 514, 909  
 Liang E., Zhang B., Dai Z. G., 2006, astro-ph/0605200  
 MacFadyen A. I., Woosley S. E., 1999, ApJ, 524, 262  
 Malesani D. et al., 2004, ApJ, 609, L5  
 Masetti N., Palazzi E., Pian E., Patat F., 2006, GCN 4803  
 Matzner C. D., McKee C. F., 1999, ApJ, 510, 379  
 Mazzali P. A., Deng J., Nomoto K., Pian E., Tominaga N., Tanaka M., Maeda K., 2006, astro-ph/0603567  
 Mazzali P. A. et al., 2005, Science, 308, 1284  
 Mirabal N., Halpern J. P., An D., Thorstensen J. R., Tern-drup D. M., 2006, astro-ph/0603686  
 Mirabal N. et al., 2003, ApJ, 595, 935  
 Modjaz M. et al., 2006, astro-ph/0603377  
 Nugis T., Lamers H. J. G. L. M., 2000, A&A, 360, 227  
 Nugis T., Lamers H. J. G. L. M., 2002, A&A, 389, 162  
 Paczyński B., 1998a, ApJ, 494, L45  
 Paczyński B., 1998b, in Gamma-Ray Bursts: 4th Huntsville Symposium, ed. C. A. Meegan, R. D. Preece, & T. M. Koshut (New York: American Institute of Physics), p. 783  
 Panaiteescu A., 2005, MNRAS, 363, 1409  
 Pian E. et al., 2006, astro-ph/0603530  
 Piran T., 2004, Rev. Mod. Phys., 76, 1143  
 Podsiadlowski Ph., Mazzali P. A., Nomoto K., Lazzati D., Cappellaro E., 2004, ApJ, 607, L17  
 Robert C., 1994, Ap&SS, 221, 137  
 Sazonov S. Yu., Lutovinov A. A., Sunyaev R. A., 2004, Nature, 430, 646  
 Schaefer B. E. et al., 2003, ApJ, 588, 387  
 Schaefer D., 1996, A&A, 309, 129  
 Schaefer D., Maeder A., 1992, A&A, 263, 129  
 Schmutz W., 1997, A&A, 321, 268  
 Smartt S. J., Vreeswijk P. M., Ramirez-Ruiz E., Gilmore G. F., Meikle W. P. S., Ferguson A. M. N., Knapen J. H., 2002, ApJ, 572, L147  
 Soderberg A. M. et al., 2006, astro-ph/0604389  
 Sollerman J., Östlin G., Fynbo J. P. U., Hjorth J., Fruchter A., Pedersen K., 2005, New Astronomy, 11, 103  
 Sollerman J. et al., 2006, astro-ph/0603495  
 Stanek et al., 2003, ApJ, 591, L17  
 Stanek et al., 2006, astro-ph/0604113  
 Tan J. C., Matzner C. D., McKee C. F., 2001, ApJ, 551, 946  
 van Paradijs J. et al., 1997, Nature, 396, 686  
 Vink J. S., de Koter A., 2005, A&A, 442, 587  
 Woosley S. E., Heger A., 2006a, ApJ, 637, 914  
 Woosley S. E., Heger A., 2006b, astro-ph/0604131  
 Woosley S. E., Heger A., Weaver T. A., 2002, Rev. Mod. Phys., 74, 1015

Yoon S.-C., Langer N., 2005, A&A, 443, 643  
 Zeh A., Klose S., Hartmann D. H., 2004, ApJ, 609, 952  
 Zhang B., Mészáros P., 2004, Int. J. Mod. Phys. A, 19, 2385

## APPENDIX A: OPTICAL DEPTH IN THE CASE OF $B = 1$

In the standard model of stellar winds the parameter  $b$  in equation (5) is often assumed to be unity. Then, the integral in equation (7) gives

$$\tau = \tau_0 \ln \left( 1 - \frac{\alpha}{y} \right)^{-1}, \quad (A1)$$

where

$$\tau_0 \equiv \frac{A}{\alpha R_*} = \frac{20}{\ln(1 - \alpha)^{-1}}. \quad (A2)$$

The ratio of the photospheric radius (at  $\tau = 2/3$ ) to the stellar core radius (at  $\tau = 20$ ) is

$$y_{\text{ph}} = \frac{\alpha}{1 - \exp(-2/3\tau_0)}, \quad (A3)$$

which approaches 1 as  $\alpha \rightarrow 1$ , and 30 as  $\alpha \rightarrow 0$ .

The corresponding surface mass density of the stellar wind is

$$\Sigma = \frac{2}{3\kappa} \frac{\alpha}{y_{\text{ph}} \ln(1 - \alpha/y_{\text{ph}})^{-1}}. \quad (A4)$$

The parameter  $\xi = |\partial \ln \tau / \partial \ln r|^{-1}$  is

$$\xi = \frac{y}{\alpha} \left( 1 - \frac{\alpha}{y} \right) \ln \left( 1 - \frac{\alpha}{y} \right)^{-1}, \quad (A5)$$

which approaches unity as  $y \rightarrow \infty$ , and zero as  $y \rightarrow \alpha$ .

The maximum radius where the shock breakout occurs (see Sec. 5) is given by

$$y_{\text{max}} = \frac{\alpha}{1 - \exp(-1/\tau_0)}. \quad (A6)$$

## APPENDIX B: SHOCK BREAKOUT FROM A STAR WITHOUT A WIND

The mass density in an outer layer of a star is described by a power law (see, e.g., Matzner & McKee 1999)

$$\rho = \rho_1 x^n, \quad (B1)$$

where  $x \equiv 1 - r/R_*$ ,  $n$  is related to the polytropic index  $\hat{\gamma}$  by  $\hat{\gamma} = 1 + 1/n$ . When  $\hat{\gamma} = 4/3$ , we have  $n = 3$ .

The opacity of the star is

$$\tau = \tau_0 x^{n+1}, \quad \tau_0 \equiv \frac{\kappa \rho_1 R_*}{n+1}. \quad (B2)$$

Near the stellar surface we have  $r \approx R_*$ , so the shock is accelerated according to equation (13) with  $m \approx M_{\text{ej}}$  and  $r \approx R_*$  (Tan, Matzner & McKee 2001).

The thickness of the shock front is

$$\Delta r_s \approx \frac{\tau_s}{\Gamma_s^2 \kappa \rho} = \xi \frac{\tau_s}{\tau} \frac{R_* x}{\Gamma_s^2}, \quad (B3)$$

where  $\xi = 1/(n+1)$ ,  $\tau_s = c/v_s$ .

The shock breakout occurs at a radius where  $\tau \approx \tau_s$ . The minimum value of  $x_{\text{br}}$ , which occurs when  $v_s \rightarrow c$ , is

$$x_{\text{min}} = \tau_0^{-1/(n+1)}, \quad (\text{B4})$$

corresponding to the maximum breakout radius  $r_{\text{max}} = R_\star(1 - x_{\text{min}})$ .

The pressure of the gas behind the shock front, measured in the frame of the shocked gas, is still given by equation (25), from which the temperature of the shock emergence can be calculated.

The total energy of radiation in the shock emergence, measured in the rest frame, is

$$E_{\text{br}} \approx 4\pi\xi F_\gamma^2 F_p \rho R_\star^3 (\Gamma_s v_s)^2 x \Big|_{r=R_{\text{br}}} . \quad (\text{B5})$$

The time-duration of the shock breakout is

$$t_{\text{br}} \approx \frac{R_\star x_{\text{br}}}{v_{s,\text{br}}} . \quad (\text{B6})$$

The input parameters include  $E_{\text{in}}$ ,  $M_{\text{ej}}$ ,  $R_\star$ ,  $\kappa$ , and  $\zeta \equiv \rho_1/\rho_\star$ , where  $\rho_\star \equiv M_{\text{ej}}/R_\star^3$ .

This paper has been typeset from a  $\text{\TeX}$ /  $\text{\LaTeX}$  file prepared by the author.